p110α-dependent hepatocyte signaling is critical for liver gene expression and its rewiring in MASLD

Marion Régnier[1,2], Arnaud Polizzi[1], Tiffany Fougeray[1], Anne Fougerat[1], Prunelle Perrier[1], Karen Anderson[3], Yannick Lippi[1], Smati Sarra[1], Céline Lukowicz [1], Frédéric Lasserre[1], Edwin Fouche[1], Marine Huillet[1], Clémence Rives[1], Blandine Tramunt[4,5], Claire Naylies[1], Géraldine Garcia[1], Elodie Rousseau-Bacquié[1], Justine Bertrand-Michel[4,6], Cécile Canlet[1], Sylvie Chevolleau-Mege[1], Laurent Debrauwer[1], Christophe Heymes[4], Rémy Burcelin[4], Thierry Levade[7], Pierre Gourdy[4,5], Walter Wahli[1,8,9], Yuna Blum[10], Laurence Gamet-Payrastre[1], Sandrine Ellero-Simatos[1], Julie Guillermet-Guibert[7], Phillip Hawkins[3], Len Stephens[3], Catherine Postic[2], Alexandra Montagner[4], Nicolas Loiseau[1*], Hervé Guillou[1*]

[1] Toxalim (Research Center in Food Toxicology), INRAE, ENVT, INP- PURPAN, UMR 1331, UPS, Université de Toulouse, Toulouse, France

[2] Université Paris Cité, Institut Cochin, CNRS, INSERM, Paris, France

[3] The Signaling Programme, The Babraham Institute, CB22 3AT Cambridge, United Kingdom

[4] Institut National de la Santé et de la Recherche Médicale (INSERM), UMR1297, Institute of Metabolic and Cardiovascular Diseases, University of Toulouse, Paul Sabatier University, Toulouse, France

[5] Diabetology department, CHU de Toulouse, Toulouse, France

[6] Metatoul-Lipidomic Facility, MetaboHUB, Institut National de la Santé et de la Recherche Médicale (INSERM), UMR1297, Institute of Metabolic and Cardiovascular Diseases, Toulouse, France

[7] Centre de Recherches en Cancérologie de Toulouse (CRCT), Inserm U1037, CNRS U5071, Université Toulouse III, Toulouse, France

[8] Lee Kong Chian School of Medicine, Nanyang Technological University Singapore, Clinical Sciences Building, 11 Mandalay Road, Singapore 308232, Singapore

[9] Center for Integrative Genomics, Université de Lausanne, Le Génopode, CH-1015 Lausanne, Switzerland

[10] Univ Rennes, CNRS, INSERM, IGDR (Institut de Génétique et Développement de Rennes) - UMR 6290, ERL U1305, F-35000 Rennes, France

*Co-corresponding authors: Nicolas Loiseau; nicolas.loiseau@inrae.fr; Hervé Guillou; herve.guillou@inrae.fr

Abstract

Insulin and other growth factors are key regulators of liver gene expression, including in metabolic diseases. Most of the phosphoinositide 3-kinase (PI3K) activity induced by insulin is dependent on PI3Kα. We used mice lacking p110α, the catalytic subunit of PI3Kα, to investigate its role in the regulation of liver gene expression in health and in Metabolic dysfunction-Associated Steatotic Liver Disease (MASLD). The absence of hepatocyte PI3Kα signaling promoted glucose intolerance in lean mice and significantly regulated liver gene expression, including insulin-sensitive genes, in *ad libitum* feeding. Some of the defective regulation of gene expression in response to hepatocyte-restricted insulin receptor deletion was related to PI3Kα signaling. In addition, though PI3Kα deletion in hepatocytes promoted insulin resistance, it was protective against steatotic liver disease in diet-induced obesity. In the absence of hepatocyte PI3Kα, the effect of diet-induced obesity on liver gene expression was significantly altered, with changes in rhythmic gene expression in liver. Altogether, this study highlights the specific role of p110α in the control of liver gene expression in physiology and in the metabolic rewiring that occurs during MASLD.

Introduction

The regulation of gene expression in response to growth factors and hormones is essential for the control of cell growth, survival, and metabolism. Activation of class I phosphonisotide-3 kinases (PI3Ks) is a critical signal transduction pathway used by cell-surface receptors to regulate intracellular events [1]. Receptors that access these signaling pathways include those that recognize growth factors and hormones such as insulin, a major regulator of metabolic homeostasis [2].

The concentration of insulin increases in response to a meal and controls the balance between fuel utilization and storage, maintaining glucose levels during fasting and feeding [3,4]. This occurs, in part, through the ability of insulin to regulate gene expression in a tissue- and cell-specific manner. There are three ways insulin can regulate gene expression via insulin receptors (IRs) [5]. Insulin binds to IRs present on the cell surface, activating their tyrosine kinase activity. This initiates a broad network of protein recruitment and phosphorylation, including the IR substrate (IRS) family, leading to activation of the PI3K pathway, as well as the Src homology and collagen (Shc) family and further activation of the Ras/MAP kinase pathway [5]. Stimulation of these pathways finally regulates transcription factors that control gene expression. Moreover, insulin-bound receptor can translocate to the nucleus to regulate gene expression [6].

Metabolic effects of insulin are generally considered to depend on the pathway involving PI3K. Class I PI3Ks synthesize the phospholipid PtdIns(3,4,5)P3 (PIP3). The increase in PIP3 concentration at the plasma membrane in response to PI3K activity triggers the recruitment of signaling molecules containing PIP3-specific Pleckstrin homology (PH) domains [1,7]. Phosphoinositide-dependent kinase (PDK) and the serine/threonine protein kinase AKT (also known as Protein Kinase B, PKB) possess PH domains able to bind PIP3. After the insulin-stimulated increase in PI3K activity, PDK and AKT translocate to the plasma membrane, leading to a local increase in their relative abundance [8,9]. At the plasma membrane, PDK phosphorylates AKT at Thr308. Additional Ser473 AKT phosphorylation dependent on mTORC2 occurs in a PI3K-dependent manner [8,10]. In the liver, insulin-induced AKT phosphorylation initiates a large number of downstream cellular responses, including

glycogen synthesis, glycolysis, and lipogenesis, as well as inhibition of gluconeogenesis [4,11–14].

PI3Ks are heterodimers composed of a regulatory subunit tightly bound to a catalytic lipid kinase subunit. PI3Ks are named based on their catalytic subunit. Among the four different types of class I PI3Ks (α, β, γ, and δ), PI3Kα and PI3Kβ are expressed in hepatocytes. They share the same regulatory subunits but their activities depend on distinct catalytic subunits [1]. Previous studies have shown that most PI3K activity induced by insulin is dependent on PI3Kα. Deletion of the PI3Kα catalytic subunit (p110α) in mouse hepatocytes reduces PIP3 generation and AKT activation upon insulin stimulation [15]. Mice lacking hepatocyte p110α show reduced insulin sensitivity and glucose tolerance, increased gluconeogenesis, and hypolipidemia that cannot be rescued by overexpression of the PI3Kβ catalytic subunit (p110β). Another report provided evidence that ablation of p110α, but not p110β, prevents hepatic steatosis associated with high fat diet (HFD)-induced obesity [16]. This protection from diet-induced steatosis is associated with decreased lipogenesis and reduced fatty acid uptake in hepatocytes. In contrast, other reports have shown that loss of p110α in hepatocytes is compensated by redundant PI3K activities dependent on p110β [17]. Moreover, low doses of a PI3Kα-selective inhibitor can successfully improve PI3Kα-related overgrowth syndrome without major metabolic effects [18,19].

In the present study, we analyzed the effect of hepatocyte p110α deletion on metabolic homeostasis in mice. Feeding is known to trigger changes in gene expression that depend both on IR-dependent and -independent processes in the liver [20,21], and physiological levels of insulin regulate a broad network of transcripts [22]. We performed an unbiased analysis to investigate the role of PI3Kα in the control of liver genome expression, including insulin-sensitive pathways in response to feeding. Obesity and type 2 diabetes are associated with metabolic dysfunction-associated steatotic liver disease (MASLD) [23], which is associated with extensive changes in hepatic signaling [24], genome expression [25–27], and metabolic pathways [27–29]. These changes include modification of the circadian liver rhythm, which occurs independently from changes in core clock gene expression [25,26,30,31]. Since the mechanisms underlying these changes are not elucidated, we also investigated the contribution of PI3Kα to the rewiring of liver gene expression and its rhythmicity that occurs in diet-induced obesity and MASLD. Taken together, our findings

show that signaling dependent on PI3Kα is critical for the regulation of liver gene expression in both health and metabolic disease.

Materials and Methods

Mice

In vivo studies were conducted under the European Union guidelines for the use and care of laboratory animals and were approved by an independent local ethics committee.

p110α$^{hep-/-}$ animals were created by mating floxed-p110α mice with C57BL/6J albumin-Cre transgenic mice to obtain albumin-Cre$^{+/-}$p110α$^{flox/flox}$ mice (i.e., p110α$^{hep-/-}$ mice). The p110α deletion was confirmed by PCR and HotStar Taq DNA Polymerase (5 U/µl, Qiagen) using two primer pairs: FE1, 5⊡- GGATGCGGTCTTTATTGTC -3⊡ and FE4, 5⊡- TGGCATGCTGCCGAATTG -3⊡; ma9, ACACACTGCATCAATGGC and a5, GCTGCCGAATTGCTAGGTAAGC. The amplification step for the floxed mice were as follows: 94°C for 3 min; followed by 20 cycles of touch down PCR comprising 94°C for 1 min, 65°C to 55°C for 1 min 30 sec, and 72°C for 1 min 30 sec; followed by 20 cycles of PCR comprising 94°C for 1 min, 55°C for 1 min 30 sec, and 72°C for 1 min 30 sec; and a final cycle of 72°C for 10 min. This reaction produced 634-bp, 544-bp, and 716-bp fragments, which represented the wild-type allele, the p110α sequence with an exon 18-19 deletion, and the floxed allele, respectively. The albumin-Cre allele was detected by PCR and HotStar Taq DNA Polymerase (5 U/µl, Qiagen) using the following primers: CreU, 5⊡-AGGTGTAGAGAAGGCACTTAG-3⊡ and CreD, 5⊡- CTAATCGCCATCTTCCAGCAGG-3⊡; G2lox7F, 5⊡-CCAATCCCTTGGTTCATGGTTGC- 3⊡ and G2lox7R, 5⊡-CGTAAGGCCCAAGGAAGTCCTGC-3⊡). Amplification conditions to confirm the presence of CRE were as follows: 95°C for 15 min; followed by 35 cycles of 94°C for 1 min, 65°C for 1 min, and 72°C for 1 min; and a final cycle of 72°C for 10 min. This reaction produced a 450-pb fragment representing the albumin-Cre allele.

Hepatocyte-specific IR knockout mice (IR$^{hep-/-}$) were generated by crossing animals carrying LoxP sites flanking the fourth exon of the IR gene (IR$^{lox/lox}$ stock number 006955; Jackson laboratory, Bar Harbor, ME, USA) with C57BL/6J mice, which specifically express CRE recombinase in the liver under the control of the transthyretin promoter (TTR-CreTam mice), as described previously [20].

Mice were housed under controlled temperature (23°C) and light (12-h light/12-h dark) conditions. All mice were males with free access to food (A04 U8220G1OR, Safe) and water. Albumin-Cre-/- floxed-p110α (p110αhep+/+) and TTR-Cre-/- floxed IR (IRhep+/+) littermates were used as controls.

In vivo experiments

High fat diet

Twelve-week-old p110α$^{hep+/+}$ and p110α$^{hep-/-}$ mice were fed a HFD with 60% calories from fat (D12492, Research Diet) or a control (CTRL) diet (D12450J, Research Diet) for 12 weeks. All mice had free access to food and water. At the end of the experiment, mice were fasted at Zeitgeber Time (ZT) 16 (with ZT0 being when the light is turned on and ZT12 when light is turned off) for 24 h or fed ad libitum prior to sacrifice. Mice were sacrificed at ZT16 (n=6-8 mice per group).

Choline-deficient high fat diet

Eight-week-old p110α$^{hep+/+}$ and p110α$^{hep-/-}$ mice were fed a choline-deficient HFD (CD-HFD) with 60% calories from fat (D05010403, Research Diet), a HFD with normal choline (A06071306, Research Diet), or a control (CTRL) diet (10% calories from fat) with normal choline (A08051501, Research Diet) for 11 weeks. Mice were sacrificed at ZT16 (n=6-8 mice per group).

Ketogenic diet

Twelve-week-old p110α$^{hep+/+}$ and p110α$^{hep-/-}$ mice were fed a CTRL diet (SAFE A04, Augy, France) containing 72.4% calories from carbohydrates, 8.3% from lipids, and 19.3% from proteins or a ketogenic diet (KD; TD.96355, Envigo, United States) containing 90.5% calories from lipids, 9.2% from proteins, and 0.3% from carbohydrates for 9 days. Mice were sacrificed at ZT16 (n=6-8 mice per group).

Fasting/high glucose

Sixteen-week-old p110α$^{hep+/+}$ and p110α$^{hep-/-}$ mice were fed a chow diet (SAFE A04, Augy, France). Half of the mice were given access to drinking water supplemented with 20% glucose (D-glucose, G8270, Sigma-Aldrich) 24 h prior to sacrifice. The other half of the mice

were fasted 12 h prior to sacrifice. Mice were sacrificed at ZT16. Eight mice of each genotype was used for each experimental condition.

Two-bottle preference assay and sucrose preference test

Mice were acclimated to cages with two bottles of water 1 week before the challenge. Mice were then given access to bottles with either water or water containing 10% sucrose (S9378, Sigma-Aldrich) and consumption measured daily for 4 days. The positions of the bottles in the cages were switched every day during the challenge. Mice were fed a chow diet (SAFE A04, Augy, France) throughout the experiment. At the end of the challenge, blood was taken from fed mice to measure the plasma FGF21 level in response to the sucrose load. Sucrose preference was determined by the difference between water intake and sucrose-containing water intake.

Fasting and fasting-refeeding

Twelve-week-old p110α$^{hep+/+}$ and p110α$^{hep-/-}$ mice were divided into three groups. One group was fed ad libitum until sacrifice, another group was fasted for 24 h from ZT16, and the third group was fasted for 24 h and then was refed for 4 h with the addition of 200 g/L glucose in water (n=6 mice/genotype/experimental condition). All mice were sacrificed at ZT16.

Circadian experiment

Twelve-week-old p110α$^{hep+/+}$ and p110α$^{hep-/-}$ mice were fed a control diet (D12450J, Research Diet) or an HFD (D12492, research diet) for 16 weeks. At the end of the experiment, mice were sacrificed at different time points: ZT0, ZT4, ZT8, ZT12, ZT16, and ZT20 (n=6/genotype/experimental condition). All mice had free access to food and water until sacrifice.

In vivo insulin signaling

Animals were fasted for 12 h from ZT0. At ZT12, the mice were anesthetized with isoflurane and ketamine (100 mg/kg body weight), followed by injection with insulin at 5 U/kg body weight (Umuline rapide, Lilly Laboratories) via the inferior vena cava. Five minutes after the injection, the liver, adipose tissue, and muscles were excised and snap-frozen in liquid nitrogen. Anesthetized fasted mice served as a control for this experiment.

Metabolic and physiological assays

Glucose, insulin, and pyruvate tolerance tests

For the glucose tolerance test, mice were fasted for 6 h and received an oral (2 g/kg body weight) glucose load (G7021, Sigma Aldrich). For the insulin tolerance test, mice were fasted for 6 h and received insulin (Umuline rapide, Lilly Laboratories) by intraperitoneal injection (0.2 U/L; 3g/kg). For the pyruvate tolerance test, mice were fasted for 24 h and received pyruvate by intraperitoneal injection (20% in NaCl; 2g/kg). For all tolerance tests, blood glucose was measured at the tail vein using an AccuCheck Performa glucometer (Roche Diagnostics) at T-15 (15 minutes before injection), T0, and 15, 30, 45, 60, 90, and 120 minutes after injection (and 150 min for pyruvate tolerance test).

Circulating glucose, ketone bodies, and other biochemical analysis

Blood glucose was measured using an Accu-Chek Go glucometer (Roche Diagnostics). The β-hydroxybutyrate content was measured at different fasting time points using Optium β-ketone test strips carrying Optium Xceed sensors (Abbott Diabetes Care). Aspartate transaminase (AST), alanine transaminase (ALT), free fatty acids (FFAs), triglycerides, total cholesterol, LDL cholesterol, and HDL cholesterol levels were determined from plasma samples using a COBASMIRA+ biochemical analyzer (Anexplo facility).

ELISA

Plasma FGF21 and insulin were assayed using the rat/mouse FGF21 ELISA kit (EMD Millipore) and the ultrasensitive mouse insulin ELISA kit (Crystal Chem), respectively, following the manufacturers' instructions.

Blood and tissue sampling

Prior to sacrifice, the submandibular vein was lanced and blood collected in EDTA-coated tubes (BD Microtainer, K2E tubes). Plasma was collected by centrifugation (1500 x g, 10 min, 4°C) and stored at -80°C. Following sacrifice by cervical dissociation, organs were removed, weighed, dissected, and used for histological analyses or snap-frozen in liquid nitrogen and stored at -80°C.

Analysis of insulin signaling in animal tissue by Western blot

Western blot analyses were conducted under different conditions. In the first experiment, mice were fasted for 12 h from ZT0 and received vena cava injections of insulin (Umulin rapide, Lilly Laboratories) at ZT12. Mice were sacrificed 5 minutes after insulin injection. In a second experiment, mice were fasted for 24 h and refed for 4 h with 200 g/L of glucose in water. Fasted mice were used as a control for each experiment. Tissues were immediately removed and homogenized in RIPA buffer by sonication (50 mM Tris HCl, pH 7.4, 150 mM NaCl, 2 mM EDTA, 0.1% SDS, 1 mM PMSF, 1% NP40, 0.25% sodium deoxycholate, proteinase, and phosphatase inhibitors). Particulates were removed by centrifugation at 13,000 g for 30 min. The protein concentration in each lysate was measured using a BC Assay Protein Quantitation Kit (Interchim).

Proteins were separated by SDS-polyacrylamide gel electrophoresis and transferred to a nitrocellulose membrane. Immunodetection was performed using the relevant primary antibody overnight at 4°C: anti-pSer473Akt (4058), anti-pThr308Akt (2965), anti-total Akt (9272), anti-pThr389p70 S6 kinase (9205), anti-p110α (4255), anti-pSer9GSK-3β (9336), or anti-β-actin (all Cell Signaling, 1:1000 dilution). Signals were acquired using Chemidoc (Bio-Rad) and quantified by ImageJ software. Signal intensities obtained with phospho-specific antibodies were normalized to those obtained with antibodies against total proteins.

PIP3 quantification

Following the vena cava injection of insulin, the liver was dissected and snap-frozen in liquid nitrogen. Mass spectrometry was used to measure inositol lipid levels as described previously [32] using a QTRAP 4000 (AB Sciex) mass spectrometer and employing the lipid extraction and derivatization method.

Gene expression

Total cellular RNA was extracted using Tri reagent (Molecular Research Center). Total RNA samples (2 μg) were reverse-transcribed using the High-capacity cDNA Reverse Transcription Kit (Applied Biosystems) for real-time quantitative polymerase chain reaction (qPCR) analyses. The primers for Sybr Green assays are presented in Supplementary Table 1. Amplification was performed on a Stratagene Mx3005P (Agilent Technology). The qPCR data

were normalized to the level of TATA-box binding protein (TBP) mRNA and analyzed by LinRegPCR.

Microarray

Gene expression analysis was performed as previously described (Fougeray et al., 2022). Transcriptome profiling was performed at the GeT-TRIX facility (Génotoul, Génopole, Toulouse, Occitanie) using Agilent SurePrint G3 Mouse GE 8x60K (Design 074809) according to the manufacturer's instructions [33–35]. For each sample, cyanine-3 (Cy3) labeled cRNA was prepared from 200 ng of total RNA using the One-Color Quick Amp Labeling kit (Agilent) according to the manufacturer's instructions, followed by Agencourt RNAClean XP (Agencourt Bioscience Corporation, Beverly, Massachusetts). Dye incorporation and cRNA yield were checked using Dopsense^{TM} 96 UV/VIS droplet reader (Trinean, Belgium). A total of 600 ng of the Cy3-labeled cRNA was hybridized on the microarray slides following the manufacturer's instructions. Immediately after washing, the slides were scanned on an Agilent G2505C Microarray Scanner using Agilent Scan Control A.8.5.1 software and the fluorescence signal extracted using Agilent Feature Extraction software v10.10.1.1 with default parameters. Microarray data and all experimental details are available in the Gene Expression Omnibus (GEO) database (GSE249340, GSE249341, GSE249343).

Histology

Paraformaldehyde-fixed, paraffin-embedded liver tissue was sliced into 3-μm-thick sections and stained with hematoxylin and eosin for histopathological analysis. The staining was visualized under a Leica DM4000 B microscope equipped with a Leica DFC450 C camera.

1H-NMR based metabolomics

Metabolomic profiling was performed as described previously [36]. All ^{1}H-NMR spectra were obtained on a Bruker DRX-600-Avance NMR spectrometer (Bruker, Wissembourg, France) using the AXIOM metabolomics platform (MetaToul) operating at 600.13 MHz for the ^{1}H resonance frequency and an inverse detection 5-mm [1]H-[13]C-^{15}N cryoprobe attached to a cryoplatform (the preamplifier cooling unit).

The ^{1}H-NMR spectra were acquired at 300K using a standard one-dimensional noesypr1D pulse sequence with water presaturation and a total spin-echo delay (2nτ) of 100 ms. A total

of 128 transients were collected into 64,000 data points using a spectral width of 12 ppm, relaxation delay of 2.5 s, and acquisition time of 2.28 s. The ^{1}H-^{1}H COSY, ^{1}H-^{1}H TOCSY, and ^{1}H-13C HSQC were obtained for each biological matrix in one representative sample for metabolite identification.

Data were analyzed by applying an exponential window function with 0.3-Hz line broadening prior to Fourier transformation. The resulting spectra were phased, baseline corrected, and calibrated to TSP (δ 0.00 ppm) manually using Mnova NMR (v9.0, Mestrelab Research). The spectra were subsequently imported into MatLab (R2014a, MathsWorks, Inc.). All data were analyzed using full-resolution spectra. The region containing water resonance (δ 4.6–5.2 ppm) was removed, and the spectra were normalized to the probabilistic quotient [37] and aligned using a previously published function [38].

Data were mean-centered and scaled using the unit variance scaling prior to analysis with orthogonal projection on latent structure-discriminant analysis (O-PLS-DA). The 1H-NMR data were used as independent variables (X matrix) and regressed against a dummy matrix (Y matrix) indicating the class of samples. The O-PLS-derived model was evaluated for goodness of prediction (Q2Y value) using n-fold cross-validation, where n depends on the sample size. To identify metabolites responsible for discrimination between the groups, the O-PLS-DA correlation coefficients (r2) were calculated for each variable and back-scaled into a spectral domain so that the shapes of the NMR spectra and signs of the coefficients were preserved [39,40]. The weights of the variables were color-coded according to the square of the O-PLS-DA correlation coefficients. Correlation coefficients extracted from significant models were filtered so that only significant correlations above the threshold defined by Pearson's critical correlation coefficient ($P < 0.05$; $|r| > 0.7$; n=12 per group) were considered significant.

Reporter metabolite analysis

Reporter metabolite analyses were performed to investigate the metabolites affected by transcriptional changes in the absence of p110α using the PIANO package, which enriches the gene set analysis of genome-wide data by incorporating the directionality of gene expression and combining statistical hypotheses and methods in conjunction with a previously established genome-scale metabolic model of the liver, iHepatocyte2322 [41].

Liver neutral lipids analysis

Tissue samples were homogenized in methanol/5 mM EGTA (2:1, v/v) and lipids (equivalent to 2 mg of tissue) extracted according to the Bligh–Dyer method [42] with chloroform/methanol/water (2.5:2.5:2 v/v/v) in the presence of the following internal standards: glyceryl trinonadecanoate, stigmasterol, and cholesteryl heptadecanoate (Sigma). Triglycerides, free cholesterol, and cholesterol esters were analyzed by gas-liquid chromatography on a Focus Thermo Electron system equipped with a Zebron-1 Phenomenex fused-silica capillary column (5 m, 0.25 mm i.d., 0.25 mm film thickness). The oven temperature was programmed to increase from 200 to 350°C at 5°C/min, and the carrier gas was hydrogen (0.5 bar). Injector and detector temperatures were 315°C and 345°C, respectively. All of the quantitative calculations were based on the peak area ratios relative to the internal standards [43].

Liver fatty acid analysis

Fatty acid analysis was performed as previously described (Bonvallot et al., 2018). Tissue samples were weighed and homogenized using a Fastprep system (40 s) in methanol/5 mM EGTA (2:1, v/v). An aliquot corresponding to 1 mg of tissue was sampled and 2 µg TG17 (glyceryl triheptadecanoate, Sigma Aldrich, les Ulis, France) added as internal standard to verify the completeness of hydrolysis. After hydrolysis in KOH-methanol (1.5 M) for 30 min at 56°C, FAs were transmethylated with 1 mL BF3-methanol, 10% wt (60 min at 80°C). Once cooled down, 1 mL Milli-Q water and 2 mL heptane was added to the methylated FAs and the mixture manually shaken. After centrifugation (500 g, 5 min), the upper layer containing FA methyl esters (FAMEs) was transferred to a glass tube and evaporated to dryness. Heptane (200 µL) was then added and the sample transferred to a vial. FAMEs were analyzed on a TRACE 1310 gas chromatograph (Thermo Scientific, Les Ulis, France) equipped with a split-splitless injector operated in the splitless mode and a flame-ionization detector. FAMEs were separated on a FAME-WAX™ column (30 m, 0.32 mm internal diameter, 0.25 µm film thickness) from Restek (Lisses, France) using helium as carrier gas at a constant flow rate of 1.0 mL.min^{-1}. The injector temperature was set at 225°C and the oven temperature was programmed as follows: 1 min isothermal step at 130°C, from 130°C to 245°C at 2°C.min-1 and then 8 min at 245°C. FAMEs were identified by comparing sample retention

times to those of commercial standard mixtures (Menhaden oil and Food Industry FAME Mix, Restek) using Xcalibur 2.2 software (Thermo Scientific).

Liver phospholipid and sphingolipid analysis

Chemicals and reagents

The liquid chromatography solvent, acetonitrile, was HPLC-grade and purchased from Acros Organics. Ammonium formate (>99%) was supplied by Sigma Aldrich. Synthetic lipid standards (Cer d18:1/18:0, Cer d18:1/15:0, PE 12:0/12:0, PE 16:0/16:0, PC 13:0/13:0, PC 16:0/16:0, SM d18:1/18:0, SM d18:1/12:0) were purchased from Avanti Polar Lipids.

Lipid extraction

Lipids were extracted from the liver (1 mg) as described previously [44] using dichloromethane/methanol (2% acetic acid)/water (2.5:2.5:2 v/v/v). Internal standards were added (Cer d18:1/15:0, 16 ng; PE 12:0/12:0, 180 ng; PC 13:0/13:0, 16 ng; SM d18:1/12:0, 16 ng; PI 16:0/17:0, 30 ng; PS 12:0/12:0, 156.25 ng) and the solution centrifuged at 1500 rpm for 3 min. The organic phase was collected and dried under azote, then dissolved in 50 µl MeOH. Sample solutions were analyzed by an Agilent 1290 UPLC system coupled to a G6460 triple quadripole spectrometer (Agilent Technologies). MassHunter software was used for data acquisition and analysis. A Kinetex HILIC column (Phenomenex, 50 x 4.6 mm, 2.6 µm) was used for LC separation. The column temperature was maintained at 40°C. The mobile phase, A, was acetonitrile and the B phase 10 mM ammonium formate in water at pH 3.2. The gradient was as follows: 10% to 30% B in 10 min; 100% B from 10 to 12 min; and then back to 10% B at 13 min for 1 min to re-equilibrate prior to the next injection. The flow rate of the mobile phase was 0.3 ml/min, and the injection volume was 5 µl. An electrospray source was employed in positive (for Cer, PE, PC, and SM analysis) or negative ion mode (for PI and PS analysis). The collision gas was nitrogen. The needle voltage was set at +4000 V. Several scan modes were used. First, to obtain the naturally different masses of different species, we analyzed cell lipid extracts with a precursor ion scan at 184 m/z, 241 m/z, and 264 m/z for PC/SM, PI, and Cer, respectively. We performed a neutral loss scan at 141 and 87 m/z for PE and PS, respectively. The collision energy optimums for Cer, PE, PC, SM, PI, and PS were 25 eV, 20 eV, 30 eV, 25 eV, 45 eV, and 22 eV, respectively. The corresponding SRM transitions were used to quantify different phospholipid species for each class. Two 9 MRM

acquisitions were necessary due to important differences between phospholipid classes. We used QqQ Quantitative (vB.05.00) and Qualitative Analysis software (vB.04.00). All of the quantitative calculations were based on the peak area ratios relative to the internal standards [45].

Statistical analysis

Biochemical, qPCR, and phenotypic data were analyzed using GraphPad software. Differential effects were assessed on log2 transformed data by ANOVA followed by Sidak post-hoc tests. P-values <0.05 were considered significant.

Hierarchical clustering of lipid quantification data was performed using R (R Development Core Team (2022) R Core Team (2022). R: A Language and Environment for Statistical Computing. R Foundation for Statistical Computing, Vienna, Austria, https://www.R-project.org/) with the pheatmap package [46]. Hierarchical clustering on log2 transformed data was applied to the samples and lipids using 1-Pearson correlation coefficient as distance and Ward's criterion (Ward.D2) for agglomeration. All of the data represented on the heat map had adjusted P-values <0.05 for one or more comparisons performed with an analysis of variance and is scaled by row.

Microarray data were analyzed using R and Bioconductor packages (www.bioconductor.org, v 3.0) as described in GEO accession (GSE249340, GSE249341, GSE249343). Raw data (median signal intensity) were filtered, log2 transformed, corrected for batch effects (microarray washing bath), and normalized using the quantile method.

A model was fitted using the limma lmFit function considering array weights using the arrayWeights function. Pair-wise comparisons between biological conditions were applied using specific contrasts. A correction for multiple testing was applied using the Benjamini-Hochberg procedure for the false discovery rate (FDR). Probes with FDR ≤ 0.05 were considered to be differentially expressed between conditions.

Hierarchical clustering was applied to the samples and the differentially expressed probes using 1-Pearson correlation coefficient as distance and Ward's criterion for agglomeration. The clustering results are illustrated as a heatmap of the expression signals. Gene set enrichment analysis (GSEA) was performed using the ViSEAGO R package [47] with signed -log10 adjusted p-values as the score and 10,000 permutations of random sets of 101 genes:

$score = -\log_{10}(adj.\,p.\,value) * \sqrt{logFC^2}/logFC$. GO categories with a minimal size of 50, P<0.01, and log2err >0.5 were considered significant. For GO enrichment, hypergeometric tests were performed over genes selected in GO categories extracted from the org.Mm.eg.db R package version 3.17.0. against all expressed genes. P<0.05 was considered significant. Principal component analysis (PCA) was performed on unscaled log2 transformed data using the R package FactoMineR [48,49]. Circadian gene expression profiles during a 24 h period were determined with R package dryR [50].

Results

Hepatocyte *p110α* deficiency leads to a 50% decrease in PIP3 *in vivo* and altered glucose homeostasis

Hepatocyte-specific *p110α* knockout mice (*p110α^{flox/flox}*-albumin-*Cre^{+/-}* i.e. *p110α^{hep-/-}*) were generated by crossing C57Bl/6J *p110α^{flox/flox}* mice with *albumin-Cre* mice in the same genetic background (**Supplemental Fig 1**). Hepatocyte-specific *p110α* deletion was validated by PCR analysis of *p110α* floxed (*p110α^{hep+/+}*) and Albumin-Cre (Albumin-Cre^{+/-}) genes from *p110α^{hep+/+}* and *p110α^{hep-/-}* mice using DNA from different tissues (liver, white adipose tissue, brown adipose tissue, and tail; **Fig 1A**). This reaction produced 544-bp fragments specifically in the livers of *p110α^{hep-/-}* mice and corresponded to the deleted sequence.

Loss of hepatocyte *p110α* resulted in decreased insulin signaling, which was associated with an altered PIP3/PIP2 ratio in hepatocytes *in vivo* (**Fig 1B**). The *p110α^{hep+/+}* mice had a 4-fold increase in the PIP3/PIP2 ratio in hepatocytes 5 minutes after insulin stimulation, but this induction was reduced by 50% in *p110α^{hep-/-}* mice. These results are due to a remodeling of the distribution of several phosphatidylinositol species in response to insulin (**Supplement Fig 2**). In addition to a lack of p110α protein expression, *p110α^{hep-/-}* mice had a marked reduction in the phosphorylation of p-Akt ^{Ser473}, p-Akt ^{Thr308}, p-70S6 ^{Thr389} kinase, and p-GSK-3β ^{Ser9} 5 minutes after insulin stimulation (**Fig 1C**). These results support a critical role of p110α in PIP3-mediated insulin signaling.

We also confirmed that the liver-specific absence of *p110α* leads to impaired glucose tolerance and reduced insulin sensitivity after glucose and insulin loading, respectively (**Fig 1D,E**). The *p110α^{hep-/-}* mice also exhibited increased glucose production during the pyruvate tolerance test (**Fig 1F**). These results indicate that a 50% reduction in PIP3 production in

$p110\alpha^{hep-/-}$ mice is associated with marked glucose intolerance and insulin resistance. This phenotype may be due, at least in part, to defective inhibition of gluconeogenesis.

Hepatocyte p110α signaling influences liver growth and liver gene expression in response to metabolic challenges

To investigate the role of hepatocyte p110α-dependent signaling in metabolic homeostasis, we explored the effects of feeding and fasting in $p110\alpha^{hep+/+}$ and $p110\alpha^{hep-/-}$ mice. First, we observed that $p110\alpha^{hep-/-}$ mice exhibited an altered response to feeding, characterized by elevated plasma insulin levels and a reduction in liver weight (**Fig 2A**). Next, gene expression profiling revealed that 46% of genes sensitive to feeding (n=762) are dependent on p110α (**Fig 2B**). Some of these genes (n=352) are differentially expressed between fed $p110\alpha^{hep+/+}$ and $p110\alpha^{hep-/-}$ mice (FC>1.5 and P<0.05, **Fig 2C**). To further investigate the contribution of p110α to insulin signaling in fed mice, we used hepatic gene expression profiles obtained from C57BL/6J mice treated with physiological levels of insulin [22] and compared the data to the p110α-sensitive gene clusters (**Fig 2D**). We identified 33 hepatic genes that were up-regulated in the absence of p110α and are known to be repressed by insulin *in vivo*. Interestingly, we also identified 77 insulin-inducible genes that were down-regulated in fed mice lacking hepatocyte p110α.

In line with a significant role of hepatocyte p110α in the control of insulin-sensitive liver gene expression, bioinformatic analysis predicted SREBP1-c and ChREBP as the two main transcription factors altered in the absence of p110α (**Fig 2E**). In agreement, mRNA expression of *Pnpla3*, *Scd1,* and *Fsp27* was decreased in the livers of $p110\alpha^{hep-/-}$ mice when compared to their littermates (**Fig 2F**). In contrast, FOXO1 was the only transcription factor predicted to be related to increased gene expression in $p110\alpha^{hep-/-}$ mice. Among the genes for which we observed a significant increase in mRNA expression, we found hepatokines *Igfbp1*, *Igfbp2*, and *Enho*.

Finally, we performed unbiased hepatic metabolomics profiling of aqueous metabolites using ^{1}H-NMR to investigate whether transcriptomic changes were coupled with metabolomic adjustments. Analysis of discriminant metabolites revealed higher betaine and lower lactate levels in the absence of $p110\alpha$ (**Supplemental Fig 3B**). Transcriptomic and

metabolomic data were then pooled in a consensus genome-scale metabolic model called ihepatocytes. The resulting metabolic network highlighted the metabolites that were predicted to be significantly different in the absence of hepatocyte $p110\alpha$ (**Fig 2G**). This analysis corroborated previous results and underscored the critical role of p110α-dependent signaling in glycolysis, pyruvate metabolism, and *de novo* fatty acid synthesis. In agreement with this analysis, we found that palmitate (C16:0) and oleate (C18:1n-9), two major products of de novo fatty acid biosynthesis, were reduced in the livers of $p110\alpha^{hep-/-}$ mice (**Fig 2H**).

Hepatocyte p110α is dispensable for carbohydrate and fatty acid sensing by hepatocytes

Bioinformatic analysis suggested that not only SREBP1 and FOXO1, but also ChREBP, PPARγ, PPARα, and HNF4α target genes may be sensitive to the expression of p110α in hepatocytes (**Fig 2E**). ChREBP is a key regulator of carbohydrate sensing, whereas the PPARs and HNF4α are involved in fatty acid sensing. Therefore, we questionned whether hepatocyte p110α may act not only as an insulin signaling intermediate, but also in carbohydrate- and fatty acid-mediated regulation of gene expression.

To address the possible role of p110α in the regulation of ChREBP-mediated gene expression, we performed an acute glucose challenge in which mice were either fasted or fed *ad libitum* with access to chow diet and 20% glucose solution in water for 24 h. Upon glucose challenge, $p110\alpha^{hep-/-}$ mice exhibited massive hyperglycemia (**Fig 3A**) and elevated ChREBP expression and activity, as revealed by the expression of *Chrebpα*, *Chrebpβ*, and *Lpk* in response to high glucose load (**Fig 3B**). In contrast, the glucose-mediated induction of SREBP1-c target genes, including *Gck*, *Acly,* and *Fasn,* was markedly reduced in the absence of hepatocyte p110α (**Fig 3B** and **Supplemental Fig 4A**). ChREBP is also a critical regulator of FGF21 hepatic expression, which controls sweet preference *in vivo*. We therefore investigated whether hepatocyte p110α affects sweet preference using the two-bottle preference assay. Absence of hepatocyte *p110α*-dependent signaling did not alter sucrose preference or plasma glucose levels over the 4-day experimental period (**Fig 3C**). The circulating level of FGF21, which regulates sucrose intake under the control of Chrebp [51], was similarly increased in $p110\alpha^{hep+/+}$ and $p110\alpha^{hep-/-}$ mice (**Fig 3D**). Taken together, these

findings indicate that p110α is not required for ChREBP-mediated regulation of gene expression in response to dietary carbohydrates and the control of sweet preference *in vivo*.

Next, we tested whether hepatocyte p110α-dependent signaling affects fatty acid sensing using two different challenges. First, we challenged mice with fasting and refeeding. In line with the role of p110α in insulin signaling, we observed that, upon refeeding, *p110α$^{hep-/-}$* mice exhibited high plasma levels of glucose and insulin (**Fig 3E**), which were associated with a reduction in the phosphorylation of downstream targets of insulin (**Fig 3F**). During fasting, changes in liver gene expression occur in response to adipose tissue lipolysis and regulate FGF21 production and ketogenesis through PPARα [52]. Therefore, we measured the mRNA expression of representative PPARα targets in the liver, including *Vnn1, Cyp4a14,* and *Fgf21*. Fasted *p110α$^{hep-/-}$* mice had increased mRNA expression of PPARα target genes, suggesting high fatty acid influx. Moreover, refeeding inhibited PPARα activity in a similar manner in both *p110α$^{hep+/+}$* and *p110α$^{hep-/-}$* mice, indicating that hepatocyte *p110α* is not required for the inhibition of PPARα activity during refeeding (**Fig 3G** and **Supplemental Fig 4B**). In agreement, plasma acylcarnitine levels, which reflect fatty acid β-oxidation, were found similarly induced in response to fasting and inhibited by refeeding in both *p110α$^{hep+/+}$* and *p110α$^{hep-/-}$* mice (**Fig 3H**). We also tested the kinetics of glucose and ketone body levels in the transition between fasting and refeeding. Although *p110α$^{hep-/-}$* mice exhibited mild hyperglycemia 30 minutes after refeeding, ketone body levels remained similar to those of *p110α$^{hep+/+}$* mice, suggesting that refeeding rapidly inhibits liver fatty acid catabolism and ketone body production in both *p110α$^{hep+/+}$* and *p110α$^{hep-/-}$* mice (**Fig 3I**).

In the second challenge to investigate whether p110α affects liver fatty acid uptake, we fed *p110α$^{hep+/+}$* and *p110α$^{hep-/-}$* mice a KD for 9 days. Mice from both genotypes showed reduced glucose levels and increased ketone bodies (**Fig 3J**). In addition, histological staining revealed similar tissue structures in *p110α$^{hep+/+}$* and *p110α$^{hep-/-}$* mice, further indicating that the absence of *p110α* does not alter dietary fatty acid uptake and catabolism (**Fig 3K**).

Altogether, these data suggest that hepatocyte p110α deficiency significantly influences glucose homeostasis through mechanisms that are independent of the regulation of gene expression by the carbohydrate-responsive pathways mediated by ChREBP. Moreover, p110α deficiency does not alter fatty acid uptake and subsequent regulation of liver gene expression through nuclear receptors involved in fatty acid sensing, such as PPARα.

Role of hepatocyte p110α in the regulation of insulin-sensitive liver gene expression

Hepatocyte p110α is activated *via* multiple growth factors and their receptors. To evaluate the effect of hepatocyte p110α outside of its metabolic effect mediated by the upstream IR, we used an untargeted approach allowing combined analysis of gene expression in *p110α*[hep-/-] mice and mice lacking IR in hepatocytes (IRLKO mice) [20]. We applied a distribution transformation method to integrate datasets from the two gene expression analyses and found that the absence of hepatocyte IR is more influential on the liver transcriptome than the absence of p110α, as revealed by the amplitude of the response in IRLKO mice (up to 20) compared to the *p110α*[hep-/-] mice (up to 5) (**Fig 4A**). This result suggests that, in hepatocytes, p110α is not required for some of the genomic regulation downstream of IR. Consistent with previous data and in line with the role of the IR/p110α axis in the metabolic regulation of lipid biosynthesis, we found that numerous lipogenic genes (*Scd1*, *Fasn*, *Srebp1-c*, *Acly*, *Me1*, and *Gck*) are among the most commonly down-regulated genes in the absence of IR and p110α (**Fig 4A**). GSEA was used to identify the pathways associated with differentially expressed genes. In addition to lipid metabolism, which appears as the most down-regulated pathway in both genotypes, GSEA revealed two main clusters of pathways that are specific for p110α (green) and IR (blue) (**Fig 4B**). In the absence of IR, but not p110α, mice showed up-regulation of inflammatory processes, suggesting that IR regulates the inflammatory response mainly through p110α-independent signaling. In the absence of hepatocyte p110α signaling, but not IR, mice exhibited altered regulation of transcription (**Fig 4B**).

To investigate the regulation of hepatic gene expression that is dependent on IR, p110α, or both, we gathered regulated genes in an integrative metabolic representation highlighting insulin- and p110α-mediated transcription factor and target genes (**Fig 4C**). As expected, the majority of SREBP1c and FOXO1 downstream target genes are regulated through an IR/p110α-dependent axis, though the absence of IR is more influential. We also highlighted specific transcription factor/target interactions that depend almost exclusively on IR and not p110α. These pathways are related to cell proliferation (ERK, NFkB, FOXKs), lipid metabolism (HNF1α, FOXKs, Sp1), glucose metabolism (CREB, HNF6, HNF4α), and cholesterol metabolism

(FXR, SREBP2). Interestingly, we highlighted CREBH as a transcription factor regulated by p110α but that is independent of hepatocyte IR. Therefore, at the level of gene expression, hepatocyte p110α acts through both IR-dependent and IR-independent pathways to regulate metabolism through the control of gene expression.

Hepatocyte p110α deletion leads to insulin resistance dissociated from hepatic steatosis

Next, we evaluated the importance of p110α in hepatic changes that occur in the pathological context of obesity and MASLD, conditions in which the action of liver insulin is altered. For this purpose, $p110\alpha^{hep+/+}$ and $p110\alpha^{hep-/-}$ mice were fed a chow diet (CTRL) or HFD for 12 weeks. We confirmed that $p110\alpha^{hep+/+}$ and $p110\alpha^{hep-/-}$ mice fed a HFD develop marked glucose intolerance and insulin resistance (**Fig 5A,B**). After insulin injection, the glycemia in $p110\alpha^{hep-/-}$ mice remained higher over the testing period than the one of $p110\alpha^{hep+/+}$ mice fed a HFD or of $p110\alpha^{hep-/-}$ mice fed a CTRL diet (**Fig 5B**). Consistently, the fasting hyperinsulinemia observed in $p110\alpha^{hep-/-}$ mice worsened with a HFD (**Fig 5C**).

Histology in HFD-$p110\alpha^{hep+/+}$ mice confirmed the accumulation of lipid droplets in hepatocytes. In contrast, $p110\alpha^{hep-/-}$ mice are protected from HFD-induced steatosis (**Fig 5D**). In line with histological analysis, $p110\alpha^{hep-/-}$ mice fed a HFD had a reduced liver weight and triglyceride accumulation compared to $p110\alpha^{hep+/+}$ mice, without any change in the total body weight (**Fig 5E,F and Supplemental Fig 5**). This phenotype was associated with reduced plasma and hepatic cholesterol levels (**Supplemental Fig 6**) and no increase in plasma ALT, a marker of liver damage (**Fig 5G**).

Dietary choline deficiency rapidly induces hepatic steatosis without obesity. To investigate the role of dietary choline in the protective effect of p110α against liver steatosis, mice were fed a CD-HFD for 12 weeks. Interestingly, despite a reduced liver weight, $p110\alpha^{hep-/-}$ mice had no improvement in hepatic triglycerides, inflammation, ALT and AST levels upon CD-HFD feeding (Supplemental Fig **7A,D**). Therefore, the absence of liver p110α protected mice from hepatic steatosis only with HFD feeding, not when mice exposed to a choline-deficient diet that induces steatosis without obesity. This reveals that the involvement of hepatocyte p110α in liver lipid accumulation is context-specific and is likely related to obesity and type 2 diabetes induced by HFD feeding. We also investigated the hepatic lipidome profile in the

absence of *p110α* upon HFD feeding. In hierarchical clustering (**Supplemental Fig 8A**), the heatmap highlighted a predominant effect of HFD that is independent from the genotype (clusters 3 and 4), but also revealed lipidomic changes with a HFD that depend on p110α (clusters 1, 5, and 6) (**Supplemental Fig 8A**). The abundance of phosphatidyl ethanolamine 40:3 (PE40:3) and phosphatidyl choline 36:3 (PC36:3) was significantly reduced only in *p110α^hep-/-^* mice fed an HFD, suggesting that hepatocyte p110α affects phospholipid metabolism in this context (**Supplemental Fig 8B**). The abundance of PC32:1, TG51, TG55, and Cer18:0 was significantly down-regulated or up-regulated in a similar manner in *p110α^hep+/+^* and *p110α^hep-/-^* mice fed an HFD, suggesting a minor contribution of p110α to the regulation of these lipids (**Supplemental Fig 8C,D**). PE38:4 and Cer16:0 accumulated as lipotoxic lipids only in *p110α^hep+/+^* mice upon HFD feeding, and the absence of such an accumulation in *p110α^hep-/-^* mice suggests protection from hepatic steatosis in these mice (**Supplemental Fig 8E**). In contrast, cholesterol ester C18 (EC18) and PE36:1 species were more abundant in the absence of *p110α* upon HFD feeding and may be actively involved in the protection from hepatic steatosis (**Supplemental Fig 8F**). Finally, some lipids, such as C20:5n-3 and PI36:1, were increased in *p110α^hep-/-^* mice fed a CTRL diet, but the HFD erased this effect (**Supplemental Fig 8G**). To investigate whether this lipid remodeling is associated with changes in liver mRNA expression, we measured the expression of genes encoding enzymes directly involved in lipid metabolism (**Supplemental Fig 8H**). This analysis revealed that HFD feeding further highlights the effects of hepatocyte *p110α* deletion on lipid metabolism. In particular, cholesterol metabolism, which was almost unaffected in the absence of *p110α* upon being fed a CTRL diet (see **Fig 4**), representing an important pathway regulated by p110α in the context of a HFD (**Supplemental Fig 8H**). Thus, this analysis revealed that hepatocyte p110α-dependent signaling is required for lipid remodeling that occurs during diet-induced obesity.

High fat diet reveals the critical role of p110α in the regulation of hepatic gene expression

We performed genome expression analysis to provide an overview of the role of hepatocyte p110α in the context of HFD feeding. First, we demonstrated that the vast majority of changes occurring during HFD-induced obesity are dependent on hepatocyte p110α-dependent signaling (**Fig 6A**). Genome expression analysis revealed that 3054 (2167+887) of

the 3907 genes dysregulated by HFD, i.e. 78%, are dependent on p110α (FC>1.5 and P>0.05, **Fig 6A**). Notably, under physiological conditions, p110α is responsible for only 46% of the transcriptomic changes (refer to **Fig 2B**), indicating that HFD revealed the key role of p110α in regulating the liver transcriptome. Next, we grouped genes for which expression was modified by HFD exposure in *p110α^hep+/+* mice, representing more than 77% of all dysregulated genes. PCA revealed high transcriptomic distinction on dimension 2 between *p110α^hep+/+* and *p110α^hep-/-* mice exposed to an HFD, whereas patterns in the gene expression of mice fed a CTRL diet remained fairly closed (**Fig 6B**). The genes were then clustered into a heatmap that further highlighted the p110α-dependent signatures during HFD-induced obesity (**Fig 6C**). Genes from cluster 1, which were highly decreased in *p110α^hep+/+* mice fed an HFD, were enriched in transcription-relative functions (**Fig 6D**). In contrast, *p110α^hep+/+* mice fed an HFD exhibited significant upregulation of genes related to fatty acid metabolism and oxidation. Hepatokines are some of the proteins significantly altered during obesity [53], which prompted us to evaluate the contribution of p110α to hepatokine regulation during HFD-induced obesity. We confirmed that multiple hepatokines, including Enho, Igfbp2, Fgl1, and Fst, are regulated through the p110α-dependent axis, and this effect is further accentuated upon HFD feeding, suggesting that p110α interferes with alterations in the communication between the liver and periphery that occurs during HFD-induced obesity (**Supplemental Fig 9**). We also examined the effect of HFD on the expression of genes that are under the control of transcription factors regulated by insulin. The vast majority of genes were sensitive to HFD via a mechanism involving p110α, revealing that obesity boosts the capacity of p110α to relay information from liver IR for the regulation of gene expression (**Fig 6D**). Though the IR/Akt/mTORC1 axis seemed to be further altered in the absence of p110α upon HFD feeding, the RAS/MAPK pathway remained intact in the presence or absence of p110α during HFD feeding, meaning that this pathway is largely mediated by IR-dependent but p110α-independent signaling, even during obesity. Overall, these data point to the key role of p110α signaling in hepatic transcriptomic changes that occur in HFD-induced obesity.

Hepatocyte p110α-dependent signaling is critical for HFD-induced rewiring of gene expression

Obesity and diabetes affect the liver clock [26,31]. Given the major role of p110α in the control of HFD-induced changes in gene expression, we assessed the role of p110α in the rewiring of gene expression that occurs during obesity and MASLD. First, we confirmed that, despite unchanged body weight, $p110\alpha^{hep-/-}$ mice exhibited fasting hyperglycemia without an increase in liver weight and presented with similar fat depot weights upon HFD feeding (**Fig 8A**). Next, we assessed the rhythmicity of glycemia. Though $p110\alpha^{hep+/+}$ mice had relatively stable glycemia over the day when fed CTRL diet and HFD, with only a slight shift in the maximal peak from ZT8 (CTRL) to ZT12 (HFD), $p110\alpha^{hep-/-}$ mice fed a CTRL diet exhibited constant hyperglycemia over the course of the day, whereas $p110\alpha^{hep-/-}$ mice fed a HFD had high variation in the rhythmicity of glycemia (**Fig 8B**). To determine whether the absence of $p110\alpha$ modifies core clock genes in the context of HFD-induced obesity, we assessed gene expression of *Bmal1*, *Cry1*, *Per2,* and *Rev-erbα*. The absence of hepatocyte $p110\alpha$ did not modify the expression of all these markers, regardless of the condition (CTRL versus HFD), suggesting that the absence of $p110\alpha$ in hepatocytes was not sufficient to alter the core clock, which remained intact in response to HFD (**Fig 8C**). Next, to further evaluate the role of p110α as a driver of HFD-induced rewiring of gene expression, we performed an untargeted analysis of liver gene expression rhythmicity in $p110\alpha^{hep+/+}$ and $p110\alpha^{hep-/-}$ mice fed a CTRL diet or HFD analyzed using the DryR package. This analysis first revealed higher circadian rhythmicity upon HFD feeding in the absence of p110α (**Fig 8D**), which is largely explained by an excessive peak of expression at the end of light (ZT10) and dark phases (ZT22) (**Fig 8E**).

We identified six distinct clusters with specific rhythmic profiles (**Fig 8F,G**). Consistent with the aforementioned notion of an unchanged core clock, the largest cluster (cluster 1), containing 2269 genes, regrouped genes for which rhythmicity remained intact regardless of the condition and was enriched in core clock genes. The 5 other clusters highlight the role of PI3Kα-dependent signaling in liver gene expression rhythmicity. A second cluster (1092 genes) relates to genes related to RNA processing whose ryhtmicity is lost in HFD when PI3Kα-dependent signaling is intact. Cluster 3 (649 genes) contains genes related to immunity and lipid metabolism whose hepatic rhythmicity only appears in mice lacking p110α and HFD-fed. Cluster 4 (585 genes) relates to cellular processes that become rhythmic as a consequence of p110α deficiency. Cluster 5 (468 genes) is enriched in genes related to

glycoprotein modification and show ryhtmicity induced by HFD in the absence of p110α. Finally, cluster 6 (408 genes) is enriched in genes related to tissue remodeling and their rhythmicity upon HFD in the absence of p110α. Interestingly, genes that became rhythmic during HFD-induced obesity in the absence of *p110α* largely belong to immune system and fatty acid beta-oxidation, and variations in the rhythmicity of these pathways seemed to mirror feeding rhythms (**Fig 8H**). Altogether, this analysis revealed that intact hepatocyte p110α-dependent signaling impacts liver gene expression rhythmicity and its rewiring in the context of obesity and MASLD.

Discussion

The regulation of gene expression is an essential process in controlling cell growth, survival, and metabolism in response to growth factors and hormones, such as insulin. In the present study, we investigated the contribution of hepatocyte signaling dependent on the PI3Kα catalytic subunit p110α to the control of liver gene expression in health and MASLD. Using mice with hepatocyte-specific ablation of p110α, we found that p110α is responsible for 50% of insulin-mediated PIP3 production *in vivo*, which is associated with a subsequent reduction in the phosphorylation of Akt and other downstream mediators, with a profound impact on liver growth and function. Although some studies have shown that PI3Kα is entirely responsible for PIP3 production downstream of insulin [54,55], our study and others [15] reveal that hepatocyte-specific deletion of p110α leads to a significant but partial decrease in liver PIP3 production in response to insulin, suggesting that p110α is not the only mediator of insulin-dependent PIP3 production in hepatocytes [17]. Moreover, the present study suggests that hepatocyte p110α selectively phosphorylates stearoyl/arachidonoyl species of PIP2 to produce PIP3 in response to insulin.

Insulin signals *via* its membrane receptor to regulate gene expression through PI3K-dependent and -independent pathways [5,22]. To assess the contribution of p110α to the global gene regulation mediated by insulin, we took advantage of two existing gene expression databases that evaluate insulin-sensitive gene responses [22] and those mediated by its receptor in mice lacking insulin receptor in hepatocytes (IRLKO) [20]. We used these two independent gene expression analyses to define insulin-sensitive genes

dependent on IR signaling in hepatocytes. We highlighted the contribution of hepatocyte p110α to the regulation of hepatocyte gene expression dependent on direct activation of IR signaling. These genes primarly fall into the lipid biosynthetic pathway, establishing the specific role of p110α in the IR/Akt/mTORC1 axis for the transcriptional regulation of lipid metabolism by insulin.

We further explored the influence of p110α signaling on regulators of fatty acid biosynthesis. SREBP1-c [56,57] and ChREBP [58] control the transcription of genes important for adaptations to feeding, such as those encoding for rate-limiting enzymes of *de novo* lipogenesis [21]. We found that IR/p110α-mediated lipid biosynthesis is largely dependent on SREBP1-c, but not ChREBP, as ChREBP target genes and ChREBP itself are fully induced in the absence of p110α during high glucose feeding. In contrast, SREBP1-c targets failed to increase in the absence of p110α. However, we cannot exclude that other downstream lipogenic regulators activated upon mTORC1 activation could also contribute to the regulation of de novo lipogenesis. One candidate is FOXK1, which is dephosphorylated, and thereby activated, following mTORC1 activation in hepatocytes [59]. Mice with hepatocyte-specific deletion of *Foxk1* exhibit reduced lipogenic activities and increased catabolic activities, which are associated with protection from hepatic steatosis, inflammation, and fibrosis in pre-clinical MASLD models [60].

A substantial portion of the insulin-sensitive and IR-dependent genes remain unchanged in the presence or absence of p110α. This could be due to liver insulin actions on gene expression that rely on other class IA PI3Ks such as p110β [17]. In addition, IR influences gene expression through pathways that do not require PI3K signaling. For example, the RAS-MAPK pathway is influenced by IR in a signaling branch that bypass the classical PI3K/Akt pathway [61]. Moreover, IR was recently described as a direct regulator of gene transcription by translocating into the nucleus [6].

In the IR/p110α comparative analysis, we highlighted some p110α-specific effects that are not related to insulin-sensitive pathways. Class IA PI3Ks integrate signals from growth factors, cytokines, and hormones other than insulin, which could explain why the absence of p110α leads to such responses. Among the panel of transcripts exhibiting p110α-dependent regulation, we highlighted a gene network related to cyclic adenosine 3′,5′-monophosphate–responsive element-binding protein, hepatic-specific (CREBH). CREBH is a

membrane protein that is tethered to the endoplasmic reticulum (ER) that acts as a stress-sensing transcriptional regulator of energy homeostasis associated with hyperlipidemia, MASLD, and atherosclerosis [62]. Upon energy demands or stress, CREBH is processed to release an amino-terminal fragment that functions as a transcription factor for hepatic genes encoding lipid and glucose metabolic factors while the carboxyl-terminal fragment of CREBH (CREBH-C) is secreted as a hepatokine [63].

Overall, we have demonstrated the importance of p110α in liver growth, glucose homeostasis, and the regulation of liver gene expression including part of the insulin-sensitive regulations. In addition, we further evaluated the effects of p110α deficiency in the pathological context of obesity and type 2 diabetes obtained by feeding mice an HFD. Consistent with previous work from others, we confirmed that an absence of p110α protects mice from hepatic lipid accumulation while promoting severe glucose intolerance and insulin resistance [16]. However, studies performed in primary hepatocytes suggested that the absence of p110α leads to defective FFA uptake [16]. Both fasting [64] and ketogenic diet feeding [65] induce significant changes in liver gene expression through processes involving PPARα that determine fatty acid catabolism, ketone body and FGF21 production [66,67]. During fasting, hepatocytes adapt to fatty acids derived from adipose tissue lipolysis [52] while in ketogenic diet feeding fatty acids originate from the diet [68]. Our work shows that in the absence of hepatocyte p110α, fatty acid catabolism and circulating ketone bodies as well as FGF21 levels are not altered during fasting and in response to ketogenic diet. This implies that liver fatty acid uptake is not affected in the absence of p110α -dependent signaling.

Three sources of fatty acids accumulate in MASLD: free fatty acids released from adipose tissue, fatty acids from *de novo* lipogenesis and dietary fatty acids [69]. Our study highlights that *de novo* fatty acid synthesis is reduced in the absence of hepatocyte p110α while fatty acid uptake and catabolism from adipose tissue or from the diet is not modified. Therefore, protection from MASLD induced by HFD feeding likely results from reduced expression of lipogenic genes and reduced de novo synthesis dependent on SREBP1c [70,71].

Insulin regulates the PPARα activity and ketogenesis through a mechanism involving mTORC1. Mechanistically, inhibition of mTORC1 during fasting is sufficient to induce PPARα activity [72]. Moreover, the PI3K/Akt-mTORC1/S6K axis reduces the activity of NCoR1, a

transcriptional co-repressor of PPARα [73,74]. The present study demonstrates that p110α deficiency did not affect PPARα activity in feeding conditions or the capacity of refeeding to inhibit PPARα activity, despite altered phosphorylation of components downstream of insulin. These results indicate that inhibition of the p110α/Akt/mTORC1/S6K axis is not sufficient to induce PPARα activity. Thus, these findings support the notion that autonomous regulation of PPARα activity through the insulin/PI3K/Akt/mTORC1/S6K pathway is minimal compared to the induction via adipose tissue lipolysis during fasting periods [52,66,75].

Based on gene expression and lipidomic profiling, p110α is much more influential in a pathological context of HFD than under control conditions. The lipid metabolic pathway remains strongly affected upon HFD feeding in a p110α-dependent manner, which is associated with significant lipid remodeling, as revealed by the depletion of certain lipid species that massively accumulate only in fatty livers of wild-type mice. In contrast, our analysis showed an enrichment of y-linolenic acid (C18:3n-6), arachidonic acid (C20:4n-6), and eicosapentaenoate acid (C20:5n-3) in the livers of mice lacking p110α and fed an HFD when compared to wild-type animals. Interestingly, these lipid species are found at lower levels in patients with MASH compared to healthy individuals and could explain, at least in part, the phenotype of mice lacking p110α [76]. Moreover, there are numerous diet-induced models of MASLD [77,78]. We tested the effect of a choline deficient diet that efficiently induces steatosis without weigh gain. Interestingly, we found that deletion of hepatocyte p110α does not protect against steatosis in the context of CD-HFD feeding, when liver fat accumulation occurs independently from obesity. This suggests that obesity and associated insulin resistance contribute to inducing the p110α-dependent signal that promotes hepatic lipid accumulation.

Hepatocyte IR signaling is required for maintaining the rhythmicity of gene expression [20]. Therefore, we investigated whether p110α is involved in the regulation of the liver clock. First, we found that unlike genetic ablation of liver IR signaling, the deletion of hepatocyte p110α does not alter liver core clock gene expression under healthy conditions or in obesity. HFD-induced obesity was recently reported to remodel diurnal gene expression rhythmicity despite modest changes in the expression of core clock components suggesting that other clock-independent factors contribute to rhythmic liver gene expression [25,26,31]. These recent accumulation of data establishing a link between insulin signaling

components, metabolic dysfunction, and the regulation of gene rhythmicity prompted us to investigate whether hepatocyte p110α contributes to the remodeling of gene expression during HFD-induced obesity [25,26,79,80]. We show that p110α-dependent hepatocyte signaling regulates rhythmic gene expression in the liver and is critical for the rewiring of gene expression that occurs during HFD-induced obesity. The p110α-dependent changes in rhythmic liver gene expression are independent of changes in the rhythmicity of liver core clock gene expression. Our analysis identifies p110α-dependent pathways as regulators of liver rhythmicity independent of the liver clock, in health and HFD-induced MASLD.

Even though our data are insufficient to make a direct link between hepatocyte p110α and downstream SREBP1-c in the regulation of HFD-induced liver gene rhythmicity, we have highlighted the critical role of insulin-driven p110α signaling in the regulation of SREBP1-c, especially during HFD-induced obesity. Thus, SREBP1c-mediated alterations in lipogenic rhythmicity during HFD feeding depends on upstream signals from the IR/p110α signaling pathway. Consistent with this idea, we show that the rhythmicity of lipid metabolism is largely modified in the absence of p110α. The modification of *de novo* lipogenesis rhythmicity during HFD-induced obesity is linked to alterations in SREBP1-c oscillations [26] and clock communications within the liver [81]. This suggests that change in PI3Kα-dependent signaling and downstream SREBP1c activity is a key regulator of obesity-induced changes in liver gene expression rhytmicity that occur in MASLD.

In conclusion, the present underlines the role of p110α in regulating key liver functions and demonstrates that hepatocyte p110α acts downstream of liver IR at multiple levels. First, hepatocyte p110α controls a part of hepatocyte PIP3 synthesis, which is sufficient to impact non-genomic responses as well as gene expression related to insulin signaling. Second, hepatocyte p110α downstream of IR and possibly other growth factor receptors is a key regulator of changes in gene expression that occur in HFD-induced MASLD, including the rewiring of gene expression rhythmicity that occurs independently of the clock.

Acknowledgments

Author contributions

Declaration of interests

The authors declare that they have no conflict of interest.

Figure legends

Figure 1 - Characterization of the hepatocyte-specific *p110α* knockout mouse model.

A PCR analysis of *p110α* floxed (*p110α^{flox/flox}*), *p110α* deleted (p110α^Δ), and Albumin-Cre (Albumin-Cre^{+/-}) genes in control (*p110α^{hep+/+}*) or liver knockout (*p110α^{hep-/-}*) mice using

genomic DNA from the liver, white adipose tissue (WAT), brown adipose tissue (BAT), and tail.

B Liver PIP3/PIP2 ratio determined by LC/MS for $p110\alpha^{hep+/+}$ and $p110\alpha^{hep-/-}$ mice that were fasted and then treated or not with insulin (5 U/kg) by vena cava injection (n=8 mice/group).

C Western blots of liver protein extracts evaluating the phosphorylation of AKT, p70S6K, and GSK3β in the mice in (B).

D-F Glucose (D), insulin (E), and pyruvate (F) tolerance tests and corresponding AUC (n= 6 mice/genotype).

Data information: In (B,D-F), data are presented as mean ± SEM. $^{\#\#}$P≤0.01 and $^{\#\#\#}$ P≤0.005 for treatment effect; **P≤0.01 and ***P≤0.005 for genotype effect.

Figure 2 - Absence of p110α-dependent signaling in hepatocytes affects liver growth, glucose homeostasis, and the regulation of liver gene expression.

A Plasma insulin and glucose levels and relative liver weights in $p110\alpha^{hep+/+}$ and $p110\alpha^{hep-/-}$ mice that were fed or fasted for 24 h and processed at ZT16 (n=6 mice/group).

B Venn diagram representing the genes regulated in a p110α-dependent manner in response to the nutritional status.

C Volcano plot representing the regulated genes in $p110\alpha^{hep-/-}$ vs. $p110\alpha^{hep+/+}$ fed mice. Green dots correspond to genes with a $Log_2FC>1.5$ but that are non-significant (NS). Blue and red dots represent significant genes with a $Log_2FC<1.5$ or >1.5, respectively.

D Left: Heatmap illustrating microarray data for liver samples from fed $p110\alpha^{hep+/+}$ and $p110\alpha^{hep-/-}$ mice. Right: Enrichment of insulin-sensitive genes as determined by Batista et al. (2019b). The color of the circle and the gene names are relative to the percentage of all identified insulin-sensitive genes within a cluster and the P-value of the hypergeometric test.

E Top list of the transcription factors up-regulated (top) and down-regulated (bottom) by $p110\alpha$ hepatocyte deletion as determined by TRRUST.

F Relative expression of *Pnpla3*, *Scd1*, *Fsp27*, *Igfbp1*, *Igfbp2*, and *Enho* measured by qPCR in the livers of $p110\alpha^{hep+/+}$ and $p110\alpha^{hep-/-}$ mice under fed conditions (n=6 mice/group).

G Profile of p110α-related metabolites based on ihepatocyte genome scale modeling visualized on an integrative representation of glycolysis, pyruvate metabolism, and fatty acid biosynthesis. Red circles represent metabolites significantly altered (P<0.01) in the absence of *p110α* in the fed state.

H Relative hepatic abundance of fatty acid methyl ester (FAME) C16:0 and C18:1n-9 determined by GC/MS.

Data information: Data are presented as mean ± SEM. ***P≤0.005 for genotype effect.

Figure 3 - Hepatocyte *p110α* is required for insulin signaling but not for glucose and fatty acid sensing.

A $p110\alpha^{hep+/+}$ and $p110\alpha^{hep-/-}$ mice were fasted or fed a chow diet supplemented with glucose (20%) in drinking water (n=8 mice/group) and the plasma glucose levels measured

B Relative liver gene expression of *Chrebp-α*, *Chrebp-β*, *Lpk*, *Gck*, *Acly,* and *Fasn* measured by qPCR in the mice in (A).

C Sucrose intake and plasma glucose levels measured daily during the sucrose preference test (10% sucrose in drinking water vs. water, 4 days) (n=23-24 mice/group).

D Plasma FGF21 measured after 4 days of the sucrose preference test.

E Plasma insulin and glucose levels in $p110\alpha^{hep+/+}$ and $p110\alpha^{hep-/-}$ mice fasted for 24 h and refed or not for 4 h with 20% glucose in drinking water (n=6 mice/group).

F Phosphorylation of AKT, p70S6K, and GSK3β determined by Western blot in the mice in (E).

G Relative liver expression of *Vnn1*, *Cyp4a14,* and *Fgf21* mRNA measured by qPCR in the mice in (E).

H Acylcarnitine levels measured in the blood of $p110\alpha^{hep+/+}$ and $p110\alpha^{hep-/-}$ mice fasted for 24 h and refed or not for 4 h with 20% glucose in drinking water (n=3 mice/group).

I Blood glucose and ketone levels measured in $p110\alpha^{hep+/+}$ and $p110\alpha^{hep-/-}$ mice successively fed, fasted (24 h), and refed for 5, 10, 15, or 30 min (n=6 mice/group).

J Blood glucose and ketone levels measured in plasma from $p110\alpha^{hep+/+}$ and $p110\alpha^{hep-/-}$ mice fed a CTRL diet or ketogenic diet (KD) (n=9-11 mice/group).

K Representative pictures of H/E staining of liver sections from the mice in (J). Scale bar, 100 μM.

Data information: In (A-D,H,J), data are presented as mean ± SEM. #P≤0.05, ##P≤0.01, and ###P≤0.005 for glucose (A,B) or sucrose effect (C,D), or diet (J) or nutritional status effect (H); *P≤0.05, **P≤0.01, and ***P≤0.005 for genotype effect.

Figure 4 - Hepatocyte p110α-mediated regulation of gene expression related to IR-dependent and IR-independent pathways.

A Correlation plot of data extracted from two distinct microarray experiments. The values used for correlation are -log10 adjusted P-value of the comparison indicated on the axis, weighted by the sign of the corresponding $\log_2 FC$ of expression for each gene.

B Correlation plot of gene set enrichment over genes presented in (A). The values used to plot the significant categories are the -log10 adjusted P-value of the comparison indicated on the axis, weighted by the sign of the corresponding normalized enrichment score. A manual annotation summarizes related GO categories when they cluster in the same area of the plot.

C Schematic overview of insulin-responsive transcription factors and downstream-regulated genes dependent on IR, p110α, or both. Genes in blue are regulated in absence of IR but not in absence of p110α. Genes in green are regulated in absence of p110α but not IR. Genes in orange are regulated by both IR and p110α.

Figure 5 - Hepatocyte _p110α_ deficiency disconnects hepatic steatosis from diabetes.
A,B Glucose (A) and insulin (B) tolerance tests and corresponding AUC for 12-week-old _p110α$^{hep+/+}$_ and _p110α$^{hep-/-}$_ mice fed a chow diet (CTRL) or HFD for 12 weeks (n=6 mice/group).
C Plasma insulin levels in 24 h-fasted _p110α$^{hep+/+}$_ and _p110α$^{hep-/-}$_ mice fed CTRL or HFD for 12 weeks.
D Representative pictures of H/E staining of liver sections. Scale bar, 100 μm.
E Body weight gain and liver weight at the end of the experiment in mice from (A).
F Liver content in triglycerides.
G Plasma ALT levels.

Data information: In all graphs, data are presented as mean ± SEM. [#]P≤0.05 and [###]P≤0.005 for diet effect; *P≤0.05 and ***P≤0.005 for genotype effect.

Figure 6 - Hepatocyte signaling dependent on p110α regulates HFD-mediated transcriptomic changes.

A Euler diagram representing the number of HFD-sensitive genes determined by microarray for each genotype of 12-week-old $p110\alpha^{hep+/+}$ and $p110\alpha^{hep-/-}$ mice fed a chow diet (CTRL) or HFD for 12 weeks (n=6 mice/group).

B Principal component analysis (PCA) of genes selected in (A) that were regulated by HFD in both genotypes.

C Heatmap with hierarchical clustering of genes presenting a >75% correlation to dimension 1 of the PCA in (B) and mean z-score for each group within each cluster.

D Enrichment in GO Biological Process categories on clusters determined in (C) and TRRUST enrichment.

E Schematic overview of insulin-responsive transcription factors and downstream-regulated genes dependent on or independent of p110α during HFD-induced obesity. Genes in blue are differentially expressed in $p110\alpha^{hep-/-}$ mice during obesity. Genes in black are similarly expressed in $p110\alpha^{hep+/+}$ and $p110\alpha^{hep-/-}$ mice fed an HFD.

Figure 7 - p110α dependent signaling is important for the rewiring of gene expression that occurs during obesity.

A Body weight, fasting plasma glucose levels, and liver, perigonadal, and subcutaneous adipose tissue relative weights in 12-week-old $p110\alpha^{hep+/+}$ and $p110\alpha^{hep-/-}$ mice fed a chow diet (CTRL) or HFD diet for 12 weeks (n=6/group).

B Plasma glucose levels in $p110\alpha^{hep+/+}$ (left) and $p110\alpha^{hep-/-}$ (right) mice fed a CTRL or HFD diet around the clock (ZT0 to ZT20).

C Relative hepatic mRNA expression levels of core clock genes and clock-controlled genes from qPCR analyzed by the Drylm function (DryR package).

D,E Analysis of circadian gene expression from microarray analysis of the liver, including the cumulative number of rhythmic genes (D) and phase distribution of rhythmic genes (E).

F Representation of the six rhythmic models identified by dryR that present a significant result in hypergeometric testing for at least one of the first level GO Biological Process categories. Each line represents a model, and each column an experimental group. When a group has no rhythmic parameter, the corresponding tile remains empty. When two groups share the same rhythmic parameters, their tiles are colored proportionally to the mean amplitude.

G Functional enrichment around the clock. Enrichment scores for the indicated functional terms are represented by the radial coordinate at the indicated time point. $p110\alpha^{hep+/+}$ mice are represented on the left and $p110\alpha^{hep-/-}$ mice on the right.

H Heatmap of the models selected in (F). The rows, one per gene, are sorted by acrophase. Data are scaled by row. The columns are sorted by hour (ZT0, 4, 8, 12, 16, 20). The right panel represents the GO biological process enrichment for each transcriptomic rhythmic profile.

Supplemental Figure legends

Supplemental Figure 1 - Schematic representation of the strategy for disrupting the $p110\alpha$ allele specifically in hepatocytes

A Organization of the $p110\alpha$ targeted locus.

B $p110\alpha$ targeting vector including the loxP sites surrounding exons 18 and 19 (length = 2 kb) and the PGK/neomycin selection cassette flanked by FRT sites and inserted between exon 19 and the second loxP site.

C Targeted $p110\alpha$ allele containing loxP sites, neomycin resistance selection cassette, and FRT sites.

D Targeted $p110\alpha$ allele following FLP recombinase-mediated deletion of the neomycin resistance selection cassette.

E Targeted $p110\alpha$ allele following CRE-mediated deletion of floxed exons 18 and 19. Intron sequences are represented by a black line. Exon sequences are represented by filled black rectangles. The loxP and FRT sequences are represented by blue and pink triangles, respectively. The position of the primers used to validate $p110\alpha$ floxed and deleted alleles by PCR are represented by green arrows. The length of the different targeted DNA fragments is written below the schematic construction.

Supplemental Figure 2 - Phosphatidyl inositol profile.

Phosphatidyl inositol, phosphatidylinositol 4-phosphate, and phosphatidyl 4,5-biphosphate distribution in liver samples from *p110α*$^{hep+/+}$ and *p110α*$^{hep-/-}$ mice after fasting or under fasted conditions and treated with insulin (5 U/kg) through inferior vena cava injection (n=8 mice/genotype/experimental condition).

Supplemental Figure 3 - Transcriptomic and metabolomic analyses of *p110α*$^{hep-/-}$ mice.

A Enrichment analysis of the genes significantly down-regulated (left) and up-regulated (right) between p110α$^{hep+/+}$ and p110α$^{hep-/-}$ under fed conditions.

B Left: Coefficient plots related to the O-PLS-DA models from 1H-nuclear magnetic resonance (NMR) discriminating between p110α$^{hep+/+}$ and p110α$^{hep-/-}$ mice under fed conditions. The figure shows the discriminant metabolites that are higher or lower in p110α$^{hep+/+}$ versus p110α$^{hep-/-}$ mice. Metabolites are color-coded according to their correlation coefficient, with red indicating a very strong positive correlation (R2 >0.65). The direction of the metabolite indicates the group with which it is positively associated, as labeled on the diagram. Right: Area under the curve of the 1H-NMR spectra was integrated for the lactate and betaine signals.

C Plasma levels of triglycerides and total, HDL, and LDL cholesterol in p110α$^{hep+/+}$ and p110α$^{hep-/-}$ mice under fed or fasted conditions (n=6 mice/group/experimental condition).

Supplemental Figure 4 - Gene expression profile of SREBP1-c and PPARα target genes.

A Relative expression of *Srebp1-c*, *Acc-α*, *Elovl6*, *Pepck,* and *G6pc* mRNA in liver tissue from p110α$^{hep+/+}$ and p110α$^{hep-/-}$ mice under fasting conditions or supplemented with 20% glucose in drinking water (n=8 mice/genotype/experimental condition).

B Expression of *Cyp4a10*, *Pdk4*, *Pparα*, *Fsp27,* and *Hmgcs2* mRNA in liver tissue from p110α$^{hep+/+}$ and p110α$^{hep-/-}$ mice under fasting conditions or supplemented with 20% glucose in drinking water (n=8 mice/genotype/experimental condition).

Supplemental Figure 5 - Clinical parameters of *p110α*$^{hep+/+}$ and *p110α*$^{hep-/-}$ mice under fed and fasted conditions.

Liver weight and plasma measurements including glucose levels, ketone bodies, free fatty acids, and cholesterol levels (total, HDL, and LDL).

Supplemental Figure 6 - Cholesterol metabolism in HFD-fed mice.

A Plasma cholesterol levels (total, HDL, and LDL) in p110α$^{hep+/+}$ and p110α$^{hep-/-}$ mice fed a CTRL diet or HFD (n=6 mice/group/experimental condition).

B Hepatic cholesterol levels in p110α$^{hep+/+}$ and p110α$^{hep-/-}$ mice fed a CTRL diet or HFD.

Supplemental Figure 7 – Protection from hepatic steatosis in absence of p110α occurs only in the context of obesity.

A Body weight and plasma glucose levels in the mice from (A)in 12-week-old p110αhep+/+ and p110αhep-/- mice fed a chow diet (CTRL) or a choline-deficient HFD (CD-HFD) for 12 weeks (n=6/genotype).

B Relative liver weight and liver triglyceride content in the mice from (A).

C Plasma ALT and AST activity and total cholesterol in the mice from (A).

E Representative pictures of H/E staining of liver sections. Scale bar, 100 μm.

Data information: In all graphs, data are presented as mean ± SEM. $^{\#}$ P≤0.05, $^{\#\#}$ P≤0.01, and $^{\#\#\#}$ P≤0.005 for diet effect; *P≤0.05, **P≤0.01, and ***P≤0.005 for genotype effect.

Supplemental Figure 8 - Lipidomic analysis of HFD-sensitive differences depending on p110α.

A Heatmap of hepatic lipid quantification in liver samples (n=6/group). Hierarchical clustering highlights seven different clusters based on the lipid levels.
B Relative abundance of phosphatidyl ethanolamine (PE) 40:3 and phosphatidyl choline (PC) 36:3 (n=6/genotype/experimental condition).
C Relative abundance of PC 32:1 and triglyceride (TG) C51 (n=6/genotype/experimental condition).
D Relative abundance of TG C55 and ceramide (Cer) C18:0 (n=6/genotype/experimental condition).
E Relative abundance of PE 38:4 and Cer C16:0 (n=6/genotype/experimental condition).
F Relative abundance of esterified cholesterol C18 and PE 36:1 (n=6/genotype/experimental condition).
G Relative abundance of fatty acid C20:5n-3 and PI 36:1.
H Differentially expressed genes involved in lipid trafficking, fatty acid metabolism, unsaturated fatty acid metabolism, lipid droplets, cholesterol metabolism, phospholipid metabolism, sphingolipid metabolism, and cannabinoid metabolism between $p110\alpha^{hep+/+}$ and $p110\alpha^{hep-/-}$ in mice fed CTRL diet (yellow) and HFD (grey), respectively.
Data information: In all graphs, data are presented as mean ± SEM. $^{\#}$ P≤0.05 for treatment effect, *P≤0.05 for genotype effect.

Supplemental Figure 9 - Hepatokine gene expression profile in HFD-fed mice.

The relative expression of Fgf21, Igfbp1, Gdf1, Enho, FetB, Igfbp2, Fgl1, Angptl6, Ctsd, Fst, and Lect2 mRNA in liver extracts from p110α$^{hep+/+}$ and p110α$^{hep-/-}$ mice fed a CTRL diet or HFD (n=6 mice/group/experimental condition).
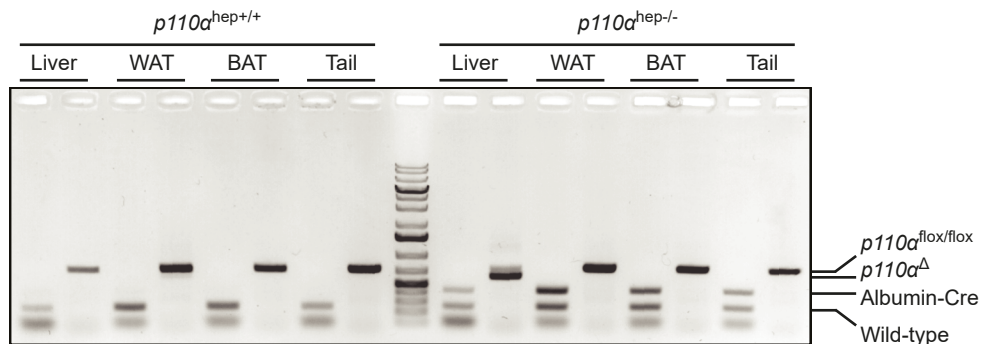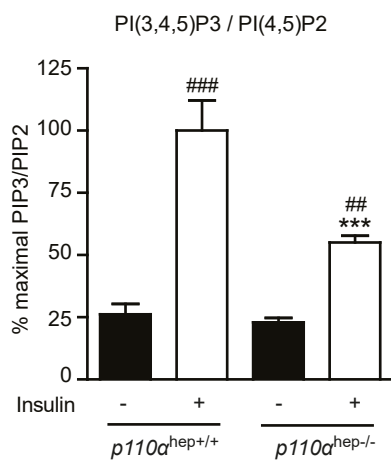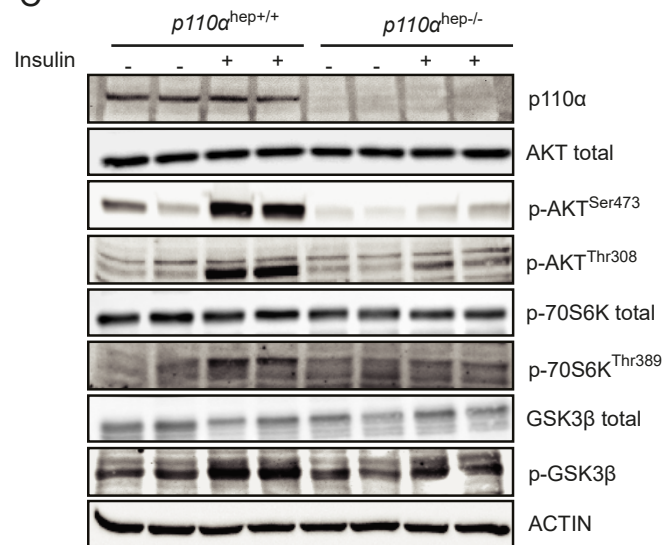
References

[1]   Hawkins PT, Anderson KE, Davidson K, Stephens LR. Signalling through Class I PI3Ks in mammalian cells. Biochem Soc Trans 2006;34:647–62. https://doi.org/10.1042/BST0340647.

[2]   White MF, Kahn CR. Insulin action at a molecular level - 100 years of progress. Mol Metab 2021;52:101304. https://doi.org/10.1016/j.molmet.2021.101304.

[3]   Roden M, Shulman GI. The integrative biology of type 2 diabetes. Nature 2019;576:51–60. https://doi.org/10.1038/s41586-019-1797-8.

[4]   Titchenell PM, Lazar MA, Birnbaum MJ. Unraveling the Regulation of Hepatic Metabolism by Insulin. Trends Endocrinol Metab 2017;28:497–505. https://doi.org/10.1016/j.tem.2017.03.003.

[5]   Batista TM, Cederquist CT, Kahn CR. The insulin receptor goes nuclear. Cell Res 2019;29:509–11. https://doi.org/10.1038/s41422-019-0185-0.

[6]   Hancock ML, Meyer RC, Mistry M, Khetani RS, Wagschal A, Shin T, et al. Insulin Receptor Associates with Promoters Genome-wide and Regulates Gene Expression. Cell 2019;177:722-736.e22. https://doi.org/10.1016/j.cell.2019.02.030.

[7]   Vanhaesebroeck B, Guillermet-Guibert J, Graupera M, Bilanges B. The emerging mechanisms of isoform-specific PI3K signalling. Nat Rev Mol Cell Biol 2010;11:329–41. https://doi.org/10.1038/nrm2882.

[8]   Manning BD, Toker A. AKT/PKB Signaling: Navigating the Network. Cell 2017;169:381–405. https://doi.org/10.1016/j.cell.2017.04.001.

[9]   Stokoe D, Stephens LR, Copeland T, Gaffney PR, Reese CB, Painter GF, et al. Dual role of phosphatidylinositol-3,4,5-trisphosphate in the activation of protein kinase B. Science 1997;277:567–70. https://doi.org/10.1126/science.277.5325.567.

[10]   Sarbassov DD, Guertin DA, Ali SM, Sabatini DM. Phosphorylation and regulation of Akt/PKB by the rictor-mTOR complex. Science 2005;307:1098–101. https://doi.org/10.1126/science.1106148.

[11]   Brown MS, Goldstein JL. Selective versus total insulin resistance: a pathogenic paradox. Cell Metab 2008;7:95–6. https://doi.org/10.1016/j.cmet.2007.12.009.

[12]   Hagiwara A, Cornu M, Cybulski N, Polak P, Betz C, Trapani F, et al. Hepatic mTORC2 activates glycolysis and lipogenesis through Akt, glucokinase, and SREBP1c. Cell Metab 2012;15:725–38. https://doi.org/10.1016/j.cmet.2012.03.015.

[13]   Li S, Brown MS, Goldstein JL. Bifurcation of insulin signaling pathway in rat liver: mTORC1 required for stimulation of lipogenesis, but not inhibition of gluconeogenesis. Proc Natl Acad Sci U S A 2010;107:3441–6. https://doi.org/10.1073/pnas.0914798107.

[14]   O-Sullivan I, Zhang W, Wasserman DH, Liew CW, Liu J, Paik J, et al. FoxO1 integrates direct and indirect effects of insulin on hepatic glucose production and glucose utilization. Nat Commun 2015;6:7079. https://doi.org/10.1038/ncomms8079.

[15]   Sopasakis VR, Liu P, Suzuki R, Kondo T, Winnay J, Tran TT, et al. Specific Roles of the p110α Isoform of Phosphatidylinsositol 3-Kinase in Hepatic Insulin Signaling and Metabolic Regulation. Cell Metabolism 2010;11:220–30. https://doi.org/10.1016/j.cmet.2010.02.002.

[16]   Chattopadhyay M, Selinger ES, Ballou LM, Lin RZ. Ablation of PI3K p110-α prevents high-fat diet-induced liver steatosis. Diabetes 2011;60:1483–92. https://doi.org/10.2337/db10-0869.

[17]   Molinaro A, Becattini B, Mazzoli A, Bleve A, Radici L, Maxvall I, et al. Insulin-Driven PI3K-AKT Signaling in the Hepatocyte Is Mediated by Redundant PI3Kα and PI3Kβ Activities and Is Promoted by RAS. Cell Metab 2019;29:1400-1409.e5. https://doi.org/10.1016/j.cmet.2019.03.010.

[18]   Canaud G, Lopez Gutierrez JC, Irvine AD, Vabres P, Hansford JR, Ankrah N, et al. Alpelisib for treatment of patients with PIK3CA-related overgrowth spectrum (PROS). Genet Med 2023;25:100969. https://doi.org/10.1016/j.gim.2023.100969.

[19] Venot Q, Blanc T, Rabia SH, Berteloot L, Ladraa S, Duong J-P, et al. Targeted therapy in patients with PIK3CA-related overgrowth syndrome. Nature 2018;558:540–6. https://doi.org/10.1038/s41586-018-0217-9.

[20] Fougeray T, Polizzi A, Régnier M, Fougerat A, Ellero-Simatos S, Lippi Y, et al. The hepatocyte insulin receptor is required to program the liver clock and rhythmic gene expression. Cell Rep 2022;39:110674. https://doi.org/10.1016/j.celrep.2022.110674.

[21] Haas JT, Miao J, Chanda D, Wang Y, Zhao E, Haas ME, et al. Hepatic insulin signaling is required for obesity-dependent expression of SREBP-1c mRNA but not for feeding-dependent expression. Cell Metab 2012;15:873–84. https://doi.org/10.1016/j.cmet.2012.05.002.

[22] Batista TM, Garcia-Martin R, Cai W, Konishi M, O'Neill BT, Sakaguchi M, et al. Multi-dimensional Transcriptional Remodeling by Physiological Insulin In Vivo. Cell Rep 2019;26:3429-3443.e3. https://doi.org/10.1016/j.celrep.2019.02.081.

[23] Rinella ME, Lazarus JV, Ratziu V, Francque SM, Sanyal AJ, Kanwal F, et al. A multisociety Delphi consensus statement on new fatty liver disease nomenclature. J Hepatol 2023:S0168-8278(23)00418-X. https://doi.org/10.1016/j.jhep.2023.06.003.

[24] Dittmann A, Kennedy NJ, Soltero NL, Morshed N, Mana MD, Yilmaz ÖH, et al. High-fat diet in a mouse insulin-resistant model induces widespread rewiring of the phosphotyrosine signaling network. Mol Syst Biol 2019;15:e8849. https://doi.org/10.15252/msb.20198849.

[25] Eckel-Mahan KL, Patel VR, de Mateo S, Orozco-Solis R, Ceglia NJ, Sahar S, et al. Reprogramming of the circadian clock by nutritional challenge. Cell 2013;155:1464–78. https://doi.org/10.1016/j.cell.2013.11.034.

[26] Guan D, Xiong Y, Borck PC, Jang C, Doulias P-T, Papazyan R, et al. Diet-Induced Circadian Enhancer Remodeling Synchronizes Opposing Hepatic Lipid Metabolic Processes. Cell 2018;174:831-842.e12. https://doi.org/10.1016/j.cell.2018.06.031.

[27] Smati S, Polizzi A, Fougerat A, Ellero-Simatos S, Blum Y, Lippi Y, et al. Integrative study of diet-induced mouse models of NAFLD identifies PPARα as a sexually dimorphic drug target. Gut 2022;71:807–21. https://doi.org/10.1136/gutjnl-2020-323323.

[28] Chella Krishnan K, Kurt Z, Barrere-Cain R, Sabir S, Das A, Floyd R, et al. Integration of Multi-omics Data from Mouse Diversity Panel Highlights Mitochondrial Dysfunction in Non-alcoholic Fatty Liver Disease. Cell Syst 2018;6:103-115.e7. https://doi.org/10.1016/j.cels.2017.12.006.

[29] Sabidó E, Wu Y, Bautista L, Porstmann T, Chang C-Y, Vitek O, et al. Targeted proteomics reveals strain-specific changes in the mouse insulin and central metabolic pathways after a sustained high-fat diet. Mol Syst Biol 2013;9:681. https://doi.org/10.1038/msb.2013.36.

[30] Guan D, Lazar MA. Circadian Regulation of Gene Expression and Metabolism in the Liver. Semin Liver Dis 2022;42:113–21. https://doi.org/10.1055/a-1792-4240.

[31] Kohsaka A, Laposky AD, Ramsey KM, Estrada C, Joshu C, Kobayashi Y, et al. High-fat diet disrupts behavioral and molecular circadian rhythms in mice. Cell Metab 2007;6:414–21. https://doi.org/10.1016/j.cmet.2007.09.006.

[32] Clark J, Anderson KE, Juvin V, Smith TS, Karpe F, Wakelam MJO, et al. Quantification of PtdInsP3 molecular species in cells and tissues by mass spectrometry. Nat Methods 2011;8:267–72. https://doi.org/10.1038/nmeth.1564.

[33] Klipper-Aurbach Y, Wasserman M, Braunspiegel-Weintrob N, Borstein D, Peleg S, Assa S, et al. Mathematical formulae for the prediction of the residual beta cell function during the first two years of disease in children and adolescents with insulin-dependent diabetes mellitus. Med Hypotheses 1995;45:486–90. https://doi.org/10.1016/0306-9877(95)90228-7.

[34] Smyth GK. Linear models and empirical bayes methods for assessing differential expression in microarray experiments. Stat Appl Genet Mol Biol 2004;3:Article3. https://doi.org/10.2202/1544-6115.1027.

[35] Szklarczyk D, Gable AL, Lyon D, Junge A, Wyder S, Huerta-Cepas J, et al. STRING v11: protein-protein association networks with increased coverage, supporting functional discovery in genome-wide experimental datasets. Nucleic Acids Res 2019;47:D607–13. https://doi.org/10.1093/nar/gky1131.

[36] Beckonert O, Keun HC, Ebbels TMD, Bundy J, Holmes E, Lindon JC, et al. Metabolic profiling, metabolomic and metabonomic procedures for NMR spectroscopy of urine, plasma, serum and tissue extracts. Nat Protoc 2007;2:2692–703. https://doi.org/10.1038/nprot.2007.376.

[37] Dieterle F, Ross A, Schlotterbeck G, Senn H. Probabilistic quotient normalization as robust method to account for dilution of complex biological mixtures. Application in 1H NMR metabonomics. Anal Chem 2006;78:4281–90. https://doi.org/10.1021/ac051632c.

[38] Veselkov KA, Lindon JC, Ebbels TMD, Crockford D, Volynkin VV, Holmes E, et al. Recursive segment-wise peak alignment of biological (1)h NMR spectra for improved metabolic biomarker recovery. Anal Chem 2009;81:56–66. https://doi.org/10.1021/ac8011544.

[39] Cloarec O, Dumas M-E, Craig A, Barton RH, Trygg J, Hudson J, et al. Statistical total correlation spectroscopy: an exploratory approach for latent biomarker identification from metabolic 1H NMR data sets. Anal Chem 2005;77:1282–9. https://doi.org/10.1021/ac048630x.

[40] Cloarec O, Dumas ME, Trygg J, Craig A, Barton RH, Lindon JC, et al. Evaluation of the orthogonal projection on latent structure model limitations caused by chemical shift variability and improved visualization of biomarker changes in 1H NMR spectroscopic metabonomic studies. Anal Chem 2005;77:517–26. https://doi.org/10.1021/ac048803i.

[41] Mardinoglu A, Shoaie S, Bergentall M, Ghaffari P, Zhang C, Larsson E, et al. The gut microbiota modulates host amino acid and glutathione metabolism in mice. Mol Syst Biol 2015;11:834. https://doi.org/10.15252/msb.20156487.

[42] Bligh EG, Dyer WJ. A rapid method of total lipid extraction and purification. Can J Biochem Physiol 1959;37:911–7. https://doi.org/10.1139/o59-099.

[43] Barrans A, Jaspard B, Barbaras R, Chap H, Perret B, Collet X. Pre-beta HDL: structure and metabolism. Biochim Biophys Acta 1996;1300:73–85. https://doi.org/10.1016/0005-2760(95)00236-7.

[44] Podechard N, Ducheix S, Polizzi A, Lasserre F, Montagner A, Legagneux V, et al. Dual extraction of mRNA and lipids from a single biological sample. Sci Rep 2018;8:7019. https://doi.org/10.1038/s41598-018-25332-9.

[45] Chiappini F, Coilly A, Kadar H, Gual P, Tran A, Desterke C, et al. Metabolism dysregulation induces a specific lipid signature of nonalcoholic steatohepatitis in patients. Sci Rep 2017;7:46658. https://doi.org/10.1038/srep46658.

[46] Kolde R. pheatmap: Pretty Heatmaps 2019.

[47] Brionne A, Juanchich A, Hennequet-Antier C. ViSEAGO: a Bioconductor package for clustering biological functions using Gene Ontology and semantic similarity. BioData Min 2019;12:16. https://doi.org/10.1186/s13040-019-0204-1.

[48] Kassambara A, Mundt F. factoextra: Extract and Visualize the Results of Multivariate Data Analyses 2020.

[49] Lê S, Josse J, Husson F. FactoMineR: An R package for multivariate analysis. Journal of Statistical Software 2008;25:1–18.

[50] Weger BD, Gobet C, David FPA, Atger F, Martin E, Phillips NE, et al. Systematic analysis of differential rhythmic liver gene expression mediated by the circadian clock and feeding rhythms. Proc Natl Acad Sci U S A 2021;118:e2015803118. https://doi.org/10.1073/pnas.2015803118.

[51] Iroz A, Montagner A, Benhamed F, Levavasseur F, Polizzi A, Anthony E, et al. A Specific ChREBP and PPARα Cross-Talk Is Required for the Glucose-Mediated FGF21 Response. Cell Rep 2017;21:403–16. https://doi.org/10.1016/j.celrep.2017.09.065.

[52] Fougerat A, Schoiswohl G, Polizzi A, Régnier M, Wagner C, Smati S, et al. ATGL-dependent white adipose tissue lipolysis controls hepatocyte PPARα activity. Cell Rep 2022;39:110910. https://doi.org/10.1016/j.celrep.2022.110910.

[53] Meex RCR, Watt MJ. Hepatokines: linking nonalcoholic fatty liver disease and insulin resistance. Nat Rev Endocrinol 2017;13:509–20. https://doi.org/10.1038/nrendo.2017.56.

[54]   Foukas LC, Claret M, Pearce W, Okkenhaug K, Meek S, Peskett E, et al. Critical role for the p110alpha phosphoinositide-3-OH kinase in growth and metabolic regulation. Nature 2006;441:366–70. https://doi.org/10.1038/nature04694.

[55]   Knight ZA, Gonzalez B, Feldman ME, Zunder ER, Goldenberg DD, Williams O, et al. A pharmacological map of the PI3-K family defines a role for p110alpha in insulin signaling. Cell 2006;125:733–47. https://doi.org/10.1016/j.cell.2006.03.035.

[56]   Horton JD, Goldstein JL, Brown MS. SREBPs: activators of the complete program of cholesterol and fatty acid synthesis in the liver. J Clin Invest 2002;109:1125–31. https://doi.org/10.1172/JCI15593.

[57]   Bo T, Gao L, Yao Z, Shao S, Wang X, Proud CG, et al. Hepatic selective insulin resistance at the intersection of insulin signaling and metabolic dysfunction-associated steatotic liver disease. Cell Metab 2024;36:947–68. https://doi.org/10.1016/j.cmet.2024.04.006.

[58]   Régnier M, Carbinatti T, Parlati L, Benhamed F, Postic C. The role of ChREBP in carbohydrate sensing and NAFLD development. Nat Rev Endocrinol 2023;19:336–49. https://doi.org/10.1038/s41574-023-00809-4.

[59]   He L, Gomes AP, Wang X, Yoon SO, Lee G, Nagiec MJ, et al. mTORC1 Promotes Metabolic Reprogramming by the Suppression of GSK3-Dependent Foxk1 Phosphorylation. Mol Cell 2018;70:949-960.e4. https://doi.org/10.1016/j.molcel.2018.04.024.

[60]   Fujinuma S, Nakatsumi H, Shimizu H, Sugiyama S, Harada A, Goya T, et al. FOXK1 promotes nonalcoholic fatty liver disease by mediating mTORC1-dependent inhibition of hepatic fatty acid oxidation. Cell Rep 2023;42:112530. https://doi.org/10.1016/j.celrep.2023.112530.

[61]   Boucher J, Kleinridders A, Kahn CR. Insulin Receptor Signaling in Normal and Insulin-Resistant States. Cold Spring Harb Perspect Biol 2014;6:a009191. https://doi.org/10.1101/cshperspect.a009191.

[62]   Nakagawa Y, Satoh A, Yabe S, Furusawa M, Tokushige N, Tezuka H, et al. Hepatic CREB3L3 controls whole-body energy homeostasis and improves obesity and diabetes. Endocrinology 2014;155:4706–19. https://doi.org/10.1210/en.2014-1113.

[63]   Kim H, Song Z, Zhang R, Davies BSJ, Zhang K. A hepatokine derived from the ER protein CREBH promotes triglyceride metabolism by stimulating lipoprotein lipase activity. Sci Signal 2023;16:eadd6702. https://doi.org/10.1126/scisignal.add6702.

[64]   Goldstein I, Baek S, Presman DM, Paakinaho V, Swinstead EE, Hager GL. Transcription factor assisted loading and enhancer dynamics dictate the hepatic fasting response. Genome Res 2017;27:427–39. https://doi.org/10.1101/gr.212175.116.

[65]   Puchalska P, Crawford PA. Multi-dimensional Roles of Ketone Bodies in Fuel Metabolism, Signaling, and Therapeutics. Cell Metab 2017;25:262–84. https://doi.org/10.1016/j.cmet.2016.12.022.

[66]   Montagner A, Polizzi A, Fouché E, Ducheix S, Lippi Y, Lasserre F, et al. Liver PPARα is crucial for whole-body fatty acid homeostasis and is protective against NAFLD. Gut 2016;65:1202–14. https://doi.org/10.1136/gutjnl-2015-310798.

[67]   Régnier M, Polizzi A, Lippi Y, Fouché E, Michel G, Lukowicz C, et al. Insights into the role of hepatocyte PPARα activity in response to fasting. Mol Cell Endocrinol 2018;471:75–88. https://doi.org/10.1016/j.mce.2017.07.035.

[68]   Badman MK, Pissios P, Kennedy AR, Koukos G, Flier JS, Maratos-Flier E. Hepatic fibroblast growth factor 21 is regulated by PPARalpha and is a key mediator of hepatic lipid metabolism in ketotic states. Cell Metab 2007;5:426–37. https://doi.org/10.1016/j.cmet.2007.05.002.

[69]   Donnelly KL, Smith CI, Schwarzenberg SJ, Jessurun J, Boldt MD, Parks EJ. Sources of fatty acids stored in liver and secreted via lipoproteins in patients with nonalcoholic fatty liver disease. J Clin Invest 2005;115:1343–51. https://doi.org/10.1172/JCI23621.

[70]   Rong S, Xia M, Vale G, Wang S, Kim C-W, Li S, et al. DGAT2 inhibition blocks SREBP-1 cleavage and improves hepatic steatosis by increasing phosphatidylethanolamine in the ER. Cell Metab 2024;36:617-629.e7. https://doi.org/10.1016/j.cmet.2024.01.011.

[71] Moon Y-A, Liang G, Xie X, Frank-Kamenetsky M, Fitzgerald K, Koteliansky V, et al. The Scap/SREBP pathway is essential for developing diabetic fatty liver and carbohydrate-induced hypertriglyceridemia in animals. Cell Metab 2012;15:240–6. https://doi.org/10.1016/j.cmet.2011.12.017.

[72] Sengupta S, Peterson TR, Laplante M, Oh S, Sabatini DM. mTORC1 controls fasting-induced ketogenesis and its modulation by ageing. Nature 2010;468:1100–4. https://doi.org/10.1038/nature09584.

[73] Jo YS, Ryu D, Maida A, Wang X, Evans RM, Schoonjans K, et al. Phosphorylation of the nuclear receptor corepressor 1 by protein kinase B switches its corepressor targets in the liver in mice. Hepatology 2015;62:1606–18. https://doi.org/10.1002/hep.27907.

[74] Kim K, Pyo S, Um SH. S6 kinase 2 deficiency enhances ketone body production and increases peroxisome proliferator-activated receptor alpha activity in the liver. Hepatology 2012;55:1727–37. https://doi.org/10.1002/hep.25537.

[75] Selen ES, Wolfgang MJ. mTORC1 activation is not sufficient to suppress hepatic PPARα signaling or ketogenesis. J Biol Chem 2021;297:100884. https://doi.org/10.1016/j.jbc.2021.100884.

[76] Puri P, Baillie RA, Wiest MM, Mirshahi F, Choudhury J, Cheung O, et al. A lipidomic analysis of nonalcoholic fatty liver disease. Hepatology 2007;46:1081–90. https://doi.org/10.1002/hep.21763.

[77] Gallage S, Avila JEB, Ramadori P, Focaccia E, Rahbari M, Ali A, et al. A researcher's guide to preclinical mouse NASH models. Nat Metab 2022;4:1632–49. https://doi.org/10.1038/s42255-022-00700-y.

[78] Vacca M, Kamzolas I, Harder LM, Oakley F, Trautwein C, Hatting M, et al. An unbiased ranking of murine dietary models based on their proximity to human metabolic dysfunction-associated steatotic liver disease (MASLD). Nat Metab 2024;6:1178–96. https://doi.org/10.1038/s42255-024-01043-6.

[79] Dang F, Sun X, Ma X, Wu R, Zhang D, Chen Y, et al. Insulin post-transcriptionally modulates Bmal1 protein to affect the hepatic circadian clock. Nat Commun 2016;7:12696. https://doi.org/10.1038/ncomms12696.

[80] Wu J, Bu D, Wang H, Shen D, Chong D, Zhang T, et al. The rhythmic coupling of Egr-1 and Cidea regulates age-related metabolic dysfunction in the liver of male mice. Nat Commun 2023;14:1634. https://doi.org/10.1038/s41467-023-36775-8.

[81] Guan D, Bae H, Zhou D, Chen Y, Jiang C, La CM, et al. Hepatocyte SREBP signaling mediates clock communication within the liver. J Clin Invest 2023;133:e163018. https://doi.org/10.1172/JCI163018.

A

$p110\alpha^{\text{hep+/+}}$

$p110\alpha^{\text{hep-/-}}$

Liver   WAT   BAT   Tail   Liver   WAT   BAT   Tail

$p110\alpha^{\text{flox/flox}}$
$p110\alpha^{\Delta}$
Albumin-Cre
Wild-type

B

PI(3,4,5)P3 / PI(4,5)P2

% maximal PIP3/PIP2

###

##
***

Insulin   −   +   −   +
$p110\alpha^{\text{hep+/+}}$ $p110\alpha^{\text{hep-/-}}$

C

$p110\alpha^{\text{hep+/+}}$ $p110\alpha^{\text{hep-/-}}$

Insulin   −   −   +   +   −   −   +   +

p110α
AKT total
p-AKT$^{\text{Ser473}}$
p-AKT$^{\text{Thr308}}$
p-70S6K total
p-70S6K$^{\text{Thr389}}$
GSK3β total
p-GSK3β
ACTIN

D

Glucose tolerance test

glycæmia (mg/dL)

**   **   **   **   ***   **

Time (min)

AUC

AUC (x1000)

hep   +/+   −/−

E

Insulin tolerance test

glycæmia (mg/dL)

**   **   *

Time (min)

AUC

AUC (x1000)

hep   +/+   −/−

F

Pyruvate tolerance test

glycæmia (mg/dL)

**   *   **   ***   ***

*

Time (min)

AUC

AUC (x1000)

***

hep   +/+   −/−

A Plasmatic insulin

Glycaemia

Liver weight / BW

B 1661 differentially expressed genes fed vs. fasted in *p110α*[hep+/+] (FC>1,5; p<0,05)

762 genes (46%) dependent on hepatocyte *p110α* (p<0,05)

C Differentially expressed genes fed vs. fasted in *p110α*[hep+/+] (FC>1,5; p<0,05)

log$_2$Fold Change *p110α*[hep-/-] vs *p110α*[hep+/+]

−log$_{10}$ adj.P.Val

Apoa4, Extl1, Gngt1, Reck, Mboat1, Acot11, Pls1, Pnpla3, Pnpla5, Sprr1a, Dntt, Gna14, Me1, Iqcg, Gm11128, Slc2a4, Scd3, Neurl2, Igfbp2, Irs2

D Expression level

Identified as 'insulin sensitive'

−log$_{10}$(p)   log$_2$FC

Enrich. score   leading genes

p110α[hep]   +/+   −/−

33: Irs2, Tango6, Gadd45g, Tuba8, Fbxo21, Igfbp1, Adgrf1, Rnd1, Terf2, Rapgef4

77: Apoa4, Extl1, Acot11, Iqcg, Slc2a4, Aqp8, Treh, Cidec, Tpmt, Slc10a2

E Transcription factors

Regulated by | in *p110α*[hep+/+]: SREBP1c, CHREBP, PPARγ, HNF4α, PPARα

in *p110α*[hep-/-]: FOXO1

−log$_{10}$ adj.P.Val

F

■ *p110α*[hep+/+]   ■ *p110α*[hep-/-]

Relative mRNA expression

Pnpla3, Scd1, Fsp27, Igfbp1, Igfbp2, Enho

G

β-D-Glucose → Glucose → Glucose-6-P → Fructose-6-P → Fructose-1,6-biP → DHAP → GAP

Lactate, Pyruvate, PEP, 3-P-D-glycerate, 1,3-biP-D-glycerate

Glycolysis

Pyruvate metabolism

Acetyl-coA → Malonyl-coA ← Malonate

Citrate

Fatty acid biosynthesis

Pyruvate → Acetyl-coA → OAA → Citrate → Aconitate → Isocitrate → Oxalosuccinate → 2-oxoglutarate → Succinate → Malate

TCA cycle

Butyryl-[acp], Hexanoyl-[acp], Octanoyl-[acp], Decanoyl-[acp], Dodecanoyl-[acp], Tetradecanoyl-[acp], Hexadecanoyl-[acp]

Hepatocyte

H C16:0

%Total liver FAME

C18:1n-9

%Total liver FAME

A Glucose

B *Chrebp-α* *Chrebp-β* *Lpk* *Gck* *Acly* *Fasn*

p110α^hep+/+   p110α^hep-/-

C Sucrose intake Sucrose intake Glycaemia

p110α^hep+/+   p110α^hep-/-

D Plasma FGF21

p110α^hep+/+   p110α^hep-/-

E Plasmatic insulin Glycaemia

p110α^hep+/+   p110α^hep-/-

F p110α^hep+/+   p110α^hep-/-

Fasted Refed Fasted Refed

p110α
AKT total
p-AKT^Ser473
p-AKT^Thr308
p70S6K
p-70S6K^Thr389
GSK3β total
p-GSK3β
ACTIN

G *Vnn1* *Cyp4a14* *Fgf21*

p110α^hep+/+   p110α^hep-/-

H Acylcarnitines

p110α^hep+/+ Fasted
p110α^hep+/+ Refed
p110α^hep-/- Fasted
p110α^hep-/- Refed

Carnitine SCAC LCAC

I Glycaemia Ketonemia

p110α^hep+/+   p110α^hep-/-

Fed Fasted 5 10 15 30
Minutes after Refeeding

J Glycaemia Ketonemia

CTRL KD

p110α^hep+/+   p110α^hep-/-

K p110α^hep+/+   p110α^hep-/-

CTRL

KD

100μm

A HFD vs CTRL

$p110\alpha^{hep+/+}$ | 2167 | 853 | 887 | $p110\alpha^{hep-/-}$

PCA

B

CTRL HFD
$p110\alpha^{hep+/+}$
$p110\alpha^{hep-/-}$

Individuals-PCA

Dim2 (18%)
Dim1 (56%)

C

CTRL HFD
$p110\alpha^{hep+/+}$
$p110\alpha^{hep-/-}$

$p110\alpha^{hep}$
+/+ —
-/- - - -

Gene expression level

CTRL HFD

1
2

D

GO biological process enrichement of clustered heatmap

−log10(p.val)
0   8   16

1
cytoplasmic translation
ribosome biogenesis
regulation of tube diameter

Regulated by: PPARα (TRRUST : 3.2e−06)

2
lipid metabolism
fatty acid oxidation
acyl−CoA metabolism
lipid transport
mitotic cell cycle
pyruvate metabolism

E

differentially expressed in $p110\alpha^{hep+/+}$ HFD vs $p110\alpha^{hep-/-}$ HFD

Ras

SOS GRB2 *Arrdc3* ↔ IR IRS PIP2 → PIP3
SHC p85 p110 PTEN
PI3K PDK1

CREBH → *Pepck; Apoa4; Apoc2 Cidec; Elovl5-6; Fgf21; G0s2* → Metabolism

Perp; p21; Bbc3
Apaf1; Ddb2; Shp p53
Lpin1; Gami; Tigar; Pltp
MDM2

HNF4α *Pepck; G6pc; Inhbe; Pklr*
Erbb3; Ripk4; Bnip3; Gjb1 Gluconeogenesis
Dolpp1; Aldh1l1; Rin3 Lipid metabolism
Pdzk1; Pla2g12b

Raf Map3k1

Ucp2; Ucp3 FOXA2
Acaa2; Eci1; Aacs
Fatty acid oxidation
Ketone body production

Akt

CREB
Pgc1-α
Pepck
Nur77 Gluconeogenesis
Nurr1

Other hepatokines
Enho; Angptl3; Postn; Tsku
Angptl6; Igf2bp3; Igf2bp4

Map2k3 Ikbkb Map4k4
Map3k14 *Map4k1*

FOXO1 *G6pc; Serpinb1; Pepck*
Igfbp1; Igfbp2; Fst

HNF6-α *Gck; Glut2*
Glucose metabolism

ERK
Fos
Sox9

NFkB
Nfkb2 + *Relb*
Tnf; Icam1; Fas
Gadd45b; Cxcl1; Ccnd1

Pepck; Aldoa; Klhdc7a HNF1α
Serpina7; Rarb; Fgb
Albumin metabolism
Lipid metabolism

mTORC1

PPARγ
Mogat1; Acly; Me1
Gpx3; Cyp8b1; Acsl1
Plin2; Cidec; Cd36; Muc1
Lipid uptake and synthesis

FoxKs
Scd1; Aff4
Tgoln1

SP1
Ghr → GHR - - →
Polb

Ccnd1; Fos

STAT5
Hnf6-α
Igf1
Igfals → Cell growth

Insr; Calm1
Ghr; Srebp1c
Metabolism
Nucleic acid biosynthesis
Cell cycle and proliferation

Fbp1; Fbxo32
Sqstm1; Nbr1
Ccnd1; Sgk1
Adgrg1; Mcam1

SREBP1c
• *Fasn; Gpam; Acly; Scd1*
Lpgat1; Mgll; Abcd3 Lipid biosynthesis
• *Hacd1; Hsd17b12*
Tecr; Acot7 MUFA biosynthesis
• *Gck; Me1; Glo1; Aldh9a1*
Acsm2; Acss2; Pdhb Glycolysis and pyruvate metabolism

E2F1
Acaca; Fasn; Scd1
Pdk4; Pfk2 Glucose metabolism and lipogenesis

FXR
Bsep; Pltp; Apoc2; Apoc3
Fmo3 Bile acids and lipoprotein and metabolism

SREBP2
Acat1; Fdps; Pmvk; Ggps1
Sqle; Dhcr7; Cyp7b1
Tm7sf2; Hsd17b12 Cholesterol metabolism
Abcb4-6-9; Cyp27a1

Cell proliferation and growth

Apoptosis
Cell death
Lipid metabolism

Cell proliferation
Apoptosis
Autophagy

Cell cycle
Lipid metabolism
Mitochondria